Special Issue Review Commentary

Journal of Physical Organic Chemistry

Received: 7 October 2009, Revised: 4 November 2009, Accepted: 15 November 2009, Published online in Wiley InterScience: 27 May 2010

(www.interscience.wiley.com) DOI 10.1002/poc.1663

Heavy atom motions and tunneling in hydrogen transfer reactions: the importance of the pre-tunneling state

Hans-Heinrich Limbach[a]*, K. Barbara Schowen[b] and Richard L. Schowen[b]

Arrhenius curves of selected hydrogen transfer reactions in organic molecules and enzymes are reviewed with the focus on systems exhibiting temperature-independent kinetic isotope effects. The latter can be rationalized in terms of a 'pre-tunneling state' which is formed from the reactants by heavy atom motions and which represents a suitable molecular configuration for tunneling to occur. Within the Bell–Limbach tunneling model, formation of the pre-tunneling state dominates the Arrhenius curves of the H and the D transfer even at higher temperatures if a large energy E_m is required to reach the pre-tunneling state. Tunneling from higher vibrational levels and the over-barrier reaction via the transition state which lead to temperature-dependent kinetic isotope effects dominate the Arrhenius curves only if E_m is small compared to the energy of the transition state. Using published data on several hydrogen transfer systems, the type of motions leading to the pre-tunneling state is explored. Among the phenomena which lead to large energies of the pre-tunneling state are (i) cleavage of hydrogen bonds or coordination bonds of the donor or acceptor atoms to molecules or molecular groups in order to allow the formation of the pre-tunneling state, (ii) the occurrence of an energetic intermediate on the reaction pathway within which tunneling takes place, and (iii) major reorganization of a molecular skeleton, requiring the excitation of specific vibrations in order to reach the pre-tunneling state. This model suggests a solution to the puzzle of Kwart's findings of temperature-independent kinetic isotope effects for hydrogen transfer in small organic molecules.

Keywords: hydrogen transfer; pre-tunneling state; transition state; tunneling

INTRODUCTION

We would like to thank the editor of this 'Symposium in print on hydrogen tunneling' in the *Journal of Physical Organic Chemistry*, Prof. R. More O'Ferrall, for the invitation to contribute this paper to the discussion of tunneling in hydrogen transfer reactions. We would like to focus on heavy atom motions preceding and during the tunneling process, and on an important state which has so far obtained little attention, i.e., the 'pre-tunneling state' which is located at the borderline between both types of heavy atom motions. This state constitutes a low-temperature analog to the transition state. Passage through the transition state generates temperature-dependent kinetic isotope effects at high temperatures, while tunneling from the pre-tunneling state generates temperature-independent kinetic isotope effects at low temperatures. This has been recognized only in recent years.

Using a selection of experimental examples of hydrogen transfers studied in our and other laboratories, we will try to identify various types of heavy-atom motions leading to the pre-tunneling state, from which some interesting conclusions about some so-far unexplained published kinetic data result.

SOME THEORETICAL ASPECTS OF HYDROGEN TUNNELING

A short history of hydrogen tunneling

The term 'tunneling' was first used within the context of microwave spectroscopic studies of ammonia. This molecule exhibits a small barrier for its inversion leading to a doubling of the vibrational states which are delocalized over both potential wells. This circumstance was recognized by Hund in 1927 and described in terms of the theory of two coupled oscillators.[1] The vibrational pairs are separated by the 'tunnel splitting' which – divided by Planck's constant – gives the 'tunnel frequency'. This type of tunneling, nowadays also called 'coherent' tunneling, is quite different from the 'incoherent' tunneling whose description is based on the tunneling of a plane wave through a barrier. This process was described theoretically in 1928 by Gamov and used to explain the temperature-independent rate constants of radioactive decay.[2] Bell realized in 1934 that incoherent tunneling could be a source for kinetic H/D isotope effects on rate constants of hydrogen and proton transfer.[3–8]

However, tunneling alone could not explain the kinetic heavy-atom isotope effects of general chemical reactions. A general theory of kinetic isotope effects was proposed by Bigeleisen and Wolfsberg[9–14] who combined the theory of isotope fractionation with Eyring's transition state theory.[15] In

* *Correspondence to: H.-H. Limbach, Institut für Chemie, Freie Universität Berlin, Takustrasse 3, Berlin D-14195, Germany.*
E-mail: limbach@chemie.fu-berlin.de

a *H.-H. Limbach*
Institut für Chemie, Freie Universität Berlin, Takustrasse 3, Berlin D-14195, Germany

b *K. B. Schowen, R. L. Schowen*
Department of Chemistry, University of Kansas, 1251 Wescoe Hall Drive, Lawrence, Kansas 66045, USA

the Bigeleisen theory, kinetic isotope effects arise mainly from the difference in the zero-point energies between the transition state and the initial state. Both zero-point vibrational energies and tunneling are consequences of the wave–quantum nature of matter. With *ab initio* computer programs, rate constants and KIEs can be calculated nowadays within the framework of Bigeleisen theory by analyzing only the vibrations of the initial reactant state and of the transition state. Bell then proposed to correct the kinetic isotope effects of hydrogen transfer reactions occurring over the barrier for tunneling through the barrier. His model was a one-dimensional one based on the simple Wentzel–Kramers–Brillouin equation for the probability of particle penetration through a barrier.[16–18]

The state of the art three decades ago has been summarized in various places. Bell's books 'The Proton in Chemistry' and 'The Tunnel Effect in Chemistry'[19,20] are still 'musts' for scientists working in this field. E. Caldin and V. Gold edited in 1975 a multi-author book 'Proton Transfer'.[21] Recently, several monographs have been published in this area of research.[22,23] In addition, various special issues have been published, e.g., the proceedings of the Faraday Symposium on proton transfer which took place in 1975 in Stirling, Scotland, in honor of R. P. Bell on the occasion of his retirement,[24] a Faraday Discussion meeting,[25] and a Bunsen Discussion meeting.[26]

The Bell tunnel correction was useful for two reasons: (i) it could be used in kinetic analyses without computer aid and (ii) it applies in cases of slow proton transfer, mainly from carbon to other heavy atoms, which can be followed using conventional kinetic methods. Typically, reactions in solution were studied around room temperature in a limited range of temperatures. However, for cases where kinetic data were available in larger temperature ranges full semiclassical tunneling calculations employing modified barriers have been performed, e.g., by Ingold *et al.*,[27] Limbach *et al.*,[28–31] Sutcliffe *et al.*[32] Other semiclassical models of single-proton abstractions have been proposed by Kuznetsov and Ulstrup[33–36] and modified by Knapp *et al.*[37] for use in enzyme reactions. Siebrand *et al.*[38,39] have proposed a golden-rule treatment of H transfer between the eigenstates of the reactants and products where low-frequency vibrations play an important role in the requisite variation of the heavy-atom distances across which tunneling occurs.

Various quantum-mechanical theories have been proposed which allow one to calculate isotopic Arrhenius curves from first principles, where tunneling is included. These theories generally start with an *ab initio* calculation of the reaction surface and use either quantum or statistical rate theories in order to calculate tunnel parameters or rate constants and kinetic isotope effects. Multidimensional coherent tunneling has been developed by Benderskii *et al.*[40–44] in order to calculate frequencies of coherent tunneling whereas 'variational transition state theory' has been used by Truhlar[45] and the 'instanton' approach by Smedarchina *et al.*[46] in order to calculate rate constants and kinetic isotope effects in the presence of incoherent tunneling.

Another problem is the theory of the transition from the coherent to the incoherent tunneling regime, especially for systems exhibiting degenerate proton transfers. For small systems of this kind coherent tunnel splittings had been observed, e.g., for malonaldehyde,[47–49] tropolone,[50] or formic acid dimer[51] in the gas phase and in low-temperature matrices. By contrast, when malonaldehyde and related systems are embedded in condensed matter, intermolecular interactions lift the gas phase symmetry of the double well leading to localized protons and incoherent tunneling.[52,53] Only in the case of exchange of dihydrogen pairs in organometallic molecules coherent tunnel splittings survive in condensed matter.[54,55] The problem of how coherent tunnel splittings mutate to rate constants was posed by J. Brickmann and H. Zimmermann[56–59] (HHL's colleague and mentor, respectively). All three writers owe them much as they motivated HHL to undertake studies of proton transfer using dynamic NMR spectroscopy.

The problem of the transition from the coherent to the incoherent regime needs a multidimensional description, for example a Redfield-relaxation-type theory as proposed by Meyer *et al.*[60] in which the coupling of the system of interest to a bath of oscillators is taken into account. The case of dihydrogen exchange has been recently reviewed.[61,62] However, all first-principle treatments of hydrogen transfer reactions require extensive theoretical work and are, generally, not available for the experimentalist in the stage where he needs to simulate his Arrhenius curves. Therefore, the use of the whole range of tunneling models and theories is justified depending on the scope of a particular study.

The shape of Arrhenius curves of hydrogen transfer reactions

In this section, we discuss the general shapes of Arrhenius curves of H and D transfer reactions. For the calculation of the curves we use the Bell–Limbach tunneling model and arbitrary parameter, but the main conclusions of this section might be equally well derived from other models. For a detailed description of the tunneling model used, the reader is referred to References [30] and [31].

Three typical situations are considered in Fig. 1, involving different reaction profiles depicted schematically at the top. The corresponding Arrhenius curves of H and D transfer and the kinetic H/D isotope effects are depicted in the center and at the bottom. The initial reactant or ground state is labeled as 'R', and the product as 'P'. The three situations differ by the value of the isotope-insensitive minimum energy E_m required to reach the pre-tunneling state, which increases from zero to 8 and then to 20 kJ mol^{-1}. We label this state by a dagger '†'. $E_d = E_d^H$ is the height of the barrier in the pre-tunneling state. The barrier is assumed to be an inverted parabola. The top of the barrier corresponds to the transition state which is usually labeled by a double dagger '‡'. In all situations the sum $E_d + E_m$ was kept constant to a value of 32 kJ mol^{-1}. The energy difference $E_d^D - E_d^H$ was also kept constant to a value of 5.6 kJ mol^{-1}. It leads to a different slope of the Arrhenius curves at high temperatures. This difference can be calculated using Bigeleisen theory via a calculation and normal mode analysis of the vibrational frequencies of the initial state and of the transition state. A possible entropy change between R and † is incorporated into the pre-exponential factor *A*. Its logarithm determines the intercept of an Arrhenius curve with the ordinate axis. We assume that within the margin of error the values of *A* are the same for the transfer of the different hydrogen isotopes. For intramolecular reactions where activation entropies are small, log (A/s^{-1}) ≈ 12.6.[30,31] This is the value used in Fig. 1. The barrier width 2*a* was set to 0.5 Å in Fig. 1a, and reduced accordingly in the other situations, keeping the curvature of the barrier constant. As the barrier for D is slightly larger than for H, one can also increase in a similar way the barrier width for the D reaction[30,31] but this correction was omitted here. Finally, the

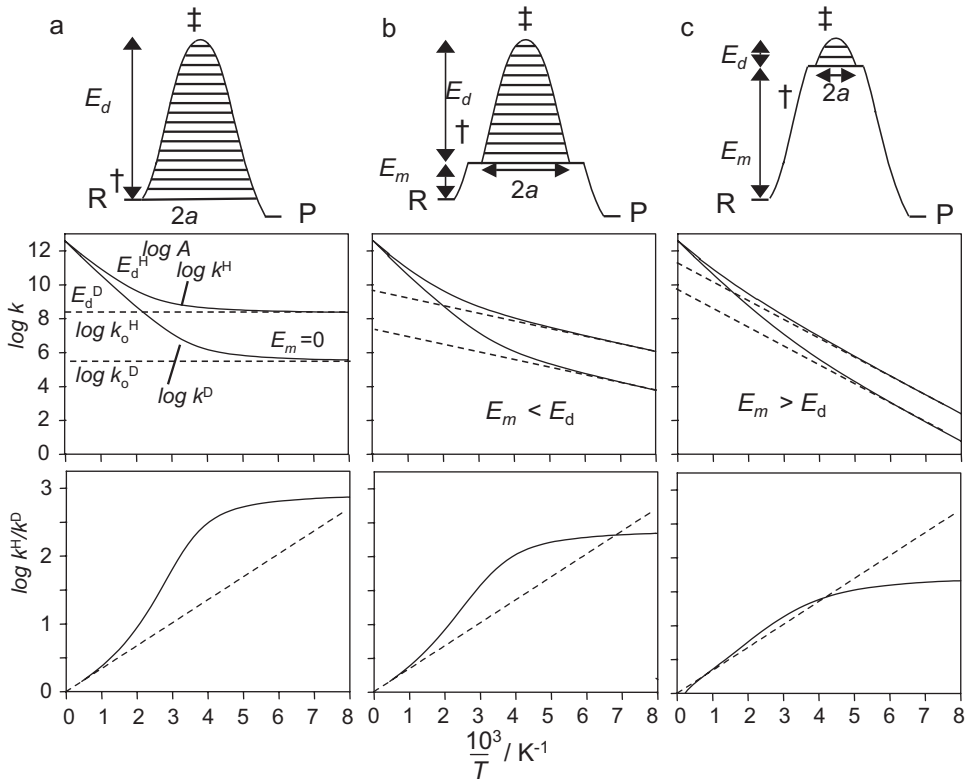

Figure 1. Schematic reaction profiles (top), Arrhenius curves (center), and temperature dependence of kinetic H/D isotope effects (bottom) of hydrogen transfer. The curves in the center and bottom panels were calculated using the Bell–Limbach tunneling model with the following values for the parameters (refer the text for definitions): $E_d + E_m = 32$ kJ mol^{-1}, $E_d^D - E_d^H = 5.6$ kJ mol^{-1}, log (A/s^{-1}) = 12.6. (a) $E_d = E_d^H = 32$ kJ mol^{-1}, $E_m = 0$, $2a = 0.5$ Å. (b) $E_d = E_d^H = 24$ kJ mol^{-1}, $E_m = 8$ kJ mol^{-1}, $2a = 0.42$ Å. (c) $E_d = E_d^H = 12$ kJ mol^{-1}, $E_m = 20$ kJ mol^{-1}, $2a = 0.3$ Å. The hatched areas in the top panel indicate the tunneling regions for values of E_m that are negligible (a), intermediate in value (b), and large (c) in comparison to E_d

tunneling masses of H and of D were set to $m^H = 1 + \Delta m$ and $m^D = 2 + \Delta m$. Δm is an additional term arising from heavy-atom motions during the tunneling process. A non-zero value of Δm reduces the kinetic isotope effects in the tunneling regime. However, for simplicity we set $\Delta m = 0$ in the calculations of the Arrhenius curves of Fig. 1. Finally, we note that these calculations are valid both in the case of degenerate as well as of non-degenerate reactions.

Figure 1a depicts the conventional case where tunneling can take place in the initial state o, i.e., where the initial state coincides with the pre-tunneling state as illustrated schematically by the harched area in the upper part of Fig. 1a. In the low-temperature limit the rate constants are independent of temperature and given by the ground-state tunneling rates k_o^H and k_o^D. The Arrhenius curves exhibit typical criteria for tunneling as formulated by Bell.[19,20] At the bottom are shown the corresponding logarithms of the kinetic H/D isotope effects which include tunneling leading to the solid line. The dashed line refers to the classical over-barrier kinetic isotope effect. At high temperatures the KIEs are entirely determined by the over-barrier reaction, but at lower temperatures the KIEs are first larger than the classical ones, but then become temperature-independent and, hence, become eventually smaller than the classical KIE.

Figure 1b depicts the case with a moderately small value of $E_m < E_d$. Essentially, similar Arrhenius curves are obtained as in Fig. 1a, but the KIEs at low temperatures are smaller, as the hatched area of the inverted barrier parabola is smaller than in Fig. 1a. The main difference is that parallel H and D Arrhenius curves are observed at low temperature.

The most interesting case is Fig. 1c where $E_m > E_d$. Now, already in a normal temperature range, parallel Arrhenius curves and temperature-independent kinetic isotope effects result, although tunneling is operative. If such data are analyzed using the Eyring equation, a slightly negative activation entropy would result as the extrapolation to high temperatures gives log k_o^H rather than log A. Surprisingly, tunneling does not lead to a particular increase of KIE, but only to smaller temperature-independent values as compared to those calculated for the over-barrier reaction.

So far, we have not yet discussed the origin of E_m, i.e., the process by which the non-reactive ground state is converted into the pre-tunneling state. In most of the cases, the heavy atoms between which H is transferred have to become close in space. The possibilities range from excitation of specific vibrational modes to complex pre-equilibria. In the latter case, the Bell–Limbach model is slightly modified as has been discussed recently in detail.[30,31] In the simplest case of a fast pre-equilibrium, the observed rate constant is given by the product

$$k_{obs} = kK \quad (1)$$

The dependence of the pre-equilibrium constant K on temperature is given by

$$K = \exp(\Delta S/R)\exp(-\Delta H/RT) \cong \exp(\Delta S/R)\exp(-E_m/RT) \quad (2)$$

where ΔH and ΔS represent the corresponding reaction enthalpy and entropy, k represents the first-order or pseudo-first order rate constant of the rate limiting H transfer in the pre-tunneling state. At high temperatures, the temperature dependence of k can be expressed by an Arrhenius law and it follows that

$$k_{obs} = A_{obs} \exp(-(E_{obs})/RT), A_{obs} = A \exp(\Delta S/R),$$
$$E_{obs} = E_m + E_d \quad (3)$$

This means that a pre-equilibrium can become manifest during the simulation of an Arrhenius curve by finding an unusual value of the observed pre-exponential factor A.

Heavy atom motions and hydrogen bond correlations

It is most obvious that in order to reach the pre-tunneling state the reactants have to come close to each other. For intermolecular reactions this has been stated by Eigen[63] in his scheme of proton transfer

$$A-H + B \overset{K}{\rightleftarrows} A-H\cdots B \overset{k}{\rightleftarrows} A\cdots H-B \rightleftarrows A+H-B \quad (4)$$

Here, the pre-equilibrium step might consist only of a diffusion-controlled reaction. However, even in the reactive complex further heavy-atom motions including excitation of specific vibrational modes might be necessary to reach the pre-tunneling state as the barrier of the transfer strongly depends on the hydrogen bond geometry. In fact, H transfers in hydrogen bonds constitute a multidimensional problem where many different modes can contribute to the reaction coordinate. Experimentally, it is not easy to identify these modes and to take them into account in simple tunneling models. There is, however, one exception: from an empirical standpoint, hydrogen bond compression has been identified as one important mode which can be taken into account using empirical hydrogen bond correlations which will be described in this section.

To any hydrogen bond A-H···B one can normally associate two distances, the A.H distance $r_1 \equiv r_{AH}$ for the diatomic unit AH and the H.B distance $r_2 \equiv r_{HB}$ for the diatomic unit HB. According to Pauling,[64,65] one can associate with these distances so-called valence bond orders or bond valences, which correspond to the 'exponential distances'

$$p_1 = \exp\{-(r_1 - r_1^o)/b_1\},\ p_2 = \exp\{-(r_2 - r_2^o)/b_2\},$$
$$\text{with } p_1 + p_2 = 1 \quad (5)$$

where b_1 and b_2 are parameters describing the decrease of the bond valences of the AH and the HB units with the corresponding distances. r_1^o and r_2^o are the equilibrium distances of the fictive non-hydrogen bonded diatomic molecules AH and HB. If one assumes that the total valence for hydrogen is unity, it follows that the two distances depend on each other, leading to an ensemble of allowed r_1 and r_2 values representing the 'geometric hydrogen bond correlation'. The hydrogen bond angle does not appear in Eqn (5). This correlation may be transformed into a correlation between the natural hydrogen bond coordinates $q_1 = \frac{1}{2}(r_1 - r_2)$ and $q_2 = r_1 + r_2$. For a linear hydrogen bond, q_1 represents the distance of H from the hydrogen bond center and q_2 the distance between atoms A and B. Experimentally, hydrogen bond correlations have been established using X-ray and neutron-diffraction crystallography,[66–68] as well as by NMR.[69] Note, however, that correlations of the type of Eqn (5) have also been used a long time ago in the context of the 'bond energy bond order' approach to describing the reaction pathway of the $H_2 + H$ reaction.[70–72] It has also been shown that the parameters in Eqn (5) can be obtained from a series of *ab initio* calculations which also provide equilibrium geometries.[73–75] Therefore, as Eqn (5) is valid only for equilibrium geometries, an empirical correction has been proposed in order to account for anharmonic zero-point vibrations.[73,76,77]

Typical equilibrium geometric hydrogen bond correlations according to Eqn (5) derived for carbon, oxygen, and nitrogen as heavy atoms are depicted in Fig. 2. When H is transferred from one heavy atom to the other, q_1 increases from negative values to positive values. q_2 goes through a minimum which is located at $q_1 = 0$ for hydrogen bonded systems of the AHA-type and near 0 for those of the AHB-type. This correlation implies that, in approximation, both proton transfer and hydrogen bonding coordinates can be combined into a single coordinate.

The shortest possible equilibrium heavy-atom distance for AHA type hydrogen bonds is given by[67]

$$q_{2\,min} = 2(r_o - b \ln 1/2) \quad (6)$$

which leads to the values for symmetric hydrogen bonds listed in Table 1. These distances provide interesting references for characterizing transition states of H-transfers obtained by quantum-mechanical calculations. For example, hydride transfer distances between two carbon atoms at the transition state were calculated to be in the range of 2.69–2.75 Å for various enzyme reactions.[78] However, the location of the pre-tunneling and transition states depends on the energy landscape schematically illustrated in Fig. 3. When the heavy-atom distance is too large, e.g., in the ground state, the barrier is also too large and tunneling is not operative. Hydrogen bond compression reduces the barrier, and tunneling is operative as illustrated by the horizontal arrows. The shortest possible hydrogen bond can, but may not, correspond to the transition state. In order to reach the pre-tunneling state the heavy-atom reorganization energy $E_m = E_r$ is required. E_r corresponds to the 'work term' in Marcus theory of electron transfer[79] and includes a molecular interpretation of the Arrhenius curve, whereas E_m might also contain, depending on the system, other contributions.

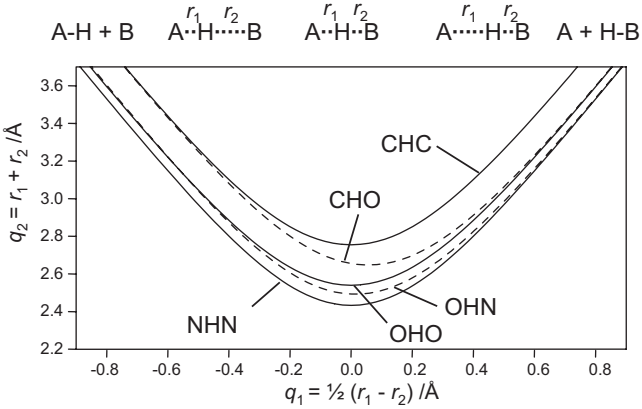

Figure 2. Correlation of the equilibrium hydrogen bond lengths $q_2 = r_1 + r_2$ with the hydrogen transfer coordinates $q_1 = \frac{1}{2}(r_1 - r_2)$ calculated using Eqn (5) and the parameters included in Table 1. Solid lines: CHC, NHN, OHO correlations. Dashed lines: CHN, NHO correlations

Table 1. Shortest possible heavy atom distances of symmetric H-bonds predicted by the valence bond order model

	r_o/Å	b/Å	q_{2min}/Å
OHO	0.95	0.37	2.41
NHN	0.99	0.404	2.53
CHC	1.1	~0.4	~2.75

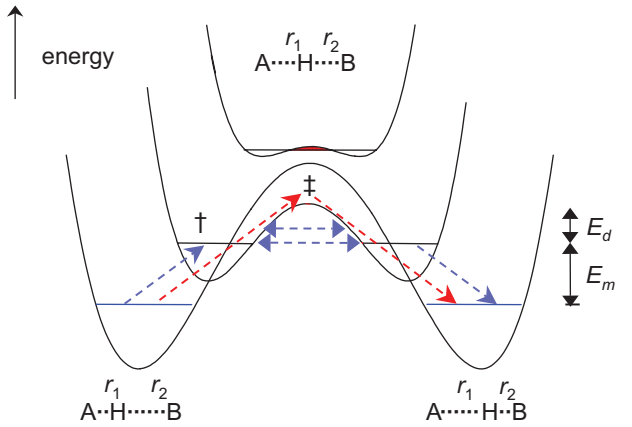

Figure 3. Effects of hydrogen bond compression on the potential of H transfer. For further explanation refer text.

EXPERIMENTAL EXAMPLES

In this section, we discuss experimental examples from our laboratory and from the literature which provide evidence that an isotope-insensitive energy E_m is necessary for the formation of the pre-tunneling state. Generally, several components may contribute to E_m, but sometimes one component can be clearly identified, e.g., hydrogen bond pre-equilibria or tunneling into a higher-energy intermediate state. More difficult to establish are combined heavy-atom motions which imply at the same time vibrational activation or conformational changes which assist the approach of heavy atoms involved in hydrogen transfer. Therefore, this section will be organized according to chemical structures rather than according to different contributions to E_m.

Hydrogen bond pre-equilibria involving solvent molecules: single H transfer in 2-hydroxyphenoxyl radicals and proton exchange between acetic acid and methanol

We discuss in this section cases of hydrogen transfers where a non-reactive species dominates, exhibiting 'wrong' hydrogen bonds. For hydrogen transfer to take place they have to be converted into reactive hydrogen bonds, which requires substantial values of E_m to reach the pre-tunneling state.

The first example is the H transfer in 2-hydroxyphenoxyl radicals which has been studied using dynamic EPR spectroscopy. When 3,6-di-*tert*-butyl-2-hydroxyphenoxyl and its deuterated analog are dissolved in heptane the Arrhenius diagram of Fig. 4 is obtained by Bubnov *et al.*[80,81] The kinetic isotope effect is about

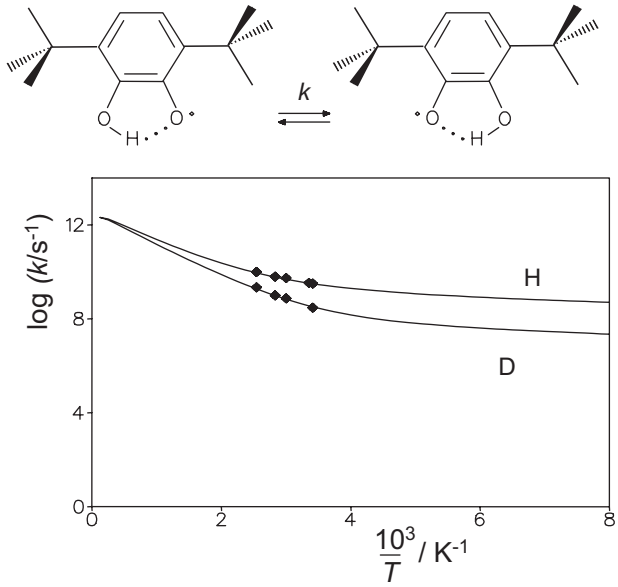

Figure 4. Arrhenius curves for the tautomerism of 3,6-di-*tert*-butyl-2-hydroxyphenoxyl in heptane. The data were taken from Bubnov *et al.*[80,81] The solid lines were calculated using the parameters listed in Table 2

10 at room temperature. Setting the pre-exponential factor to $10^{12.6}\,s^{-1}$ leads to the concave Arrhenius curves depicted as solid lines. By contrast, Fig. 5 depicts the kinetic data of the parent compound 2-hydroxyphenoxyl in CCl_4/CCl_3F to which 0.11 mol l^{-1} dioxane had been added for increasing the solubility.[82] Now, a kinetic isotope effect of about 56 is obtained at room temperature. This large difference between both molecules had been noted already some time ago by Limbach *et al.*[83] In particular, it

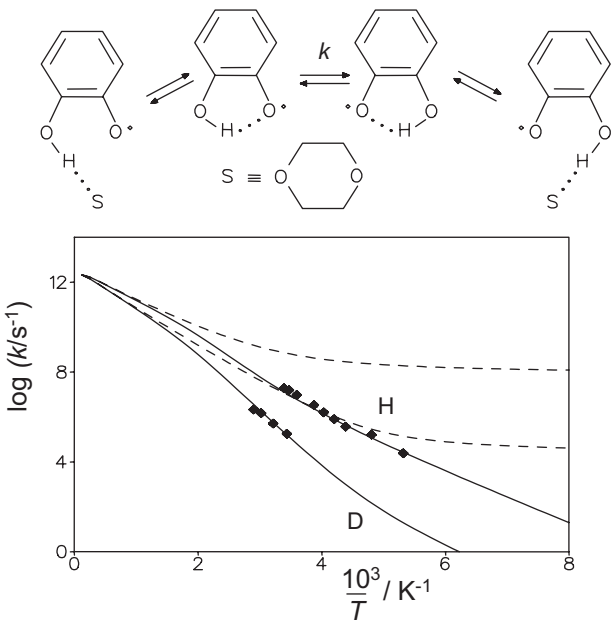

Figure 5. Arrhenius curves of the tautomerism of 2-hydroxyphenoxyl in CCl_4/CCl_3F/dioxane. The data were taken from Loth *et al.*[82] The solid lines were calculated using the parameters listed in Table 2

Journal of Physical Organic Chemistry

was noted that the two Arrhenius curves of the H and the D reaction are almost parallel.

The dashed lines in Fig. 5 indicate the intrinsic Arrhenius curves of the transfer, whereas the solid line indicates the Arrhenius curves including the pre-equilibrium. The smaller rate constants than those for the di-*tert*-butyl radical case can be explained by the formation of a non-reactive species at low temperatures which is hydrogen bonded to the added dioxane. Thus, for the reaction to occur, the intramolecularly H-bonded species has to be formed with release of dioxane, a process that should exhibit not only a higher energy requirement but also a more positive entropy. A comparison of the solid and the dashed Arrhenius curves of Fig. 5 indicates that the desolvated intramolecular H-bonded species is never the dominant species at any point in the temperature range studied, as the interaction with dioxane forms a stronger linear intermolecular H-bond, while the nonlinear intramolecular H-bond is weaker.

The larger kinetic H/D isotope effects in the parent radical can be explained in terms of the higher symmetry of the parent radical as compared to the di-*tert*-butyl radical. In the latter, the methyl groups on both sides of the ring are not ordered, leading to a distribution of asymmetric double-well potentials of the H-transfer. These examples show how subtle structural effects can lead to very different H-transfer properties.

A related solvent effect was found for the proton exchange between acetic acid and methanol in tetrahydrofuran by Bureiko *et al.*[84] and by Gerritzen *et al.*[28,29] Hydrogen bonding to the solvent prevents the formation of the cyclic complexes in which the proton exchange takes place. Unfortunately, these complexes could not be seen directly. The rate constants were measured as a function of concentration. At low concentration, a second-order rate law was obtained indicating a HH transfer in a cyclic 1:1 hydrogen bonded complex between acetic acid and methanol. At higher concentrations, the rate law changed, indicating the participation of two acetic acid molecules, i.e., a HHH process. The multiple kinetic isotope effects are shown as a function of the inverse temperature in Fig. 6.

For the double proton transfer (Fig. 6a) two large kinetic HH/HD and HD/DD isotope effects of about 5 and 3 were observed. Recently, this reaction has been modeled using the instanton approach by Fernández-Ramos *et al.*[85] The Arrhenius curves could be reproduced. In the transition state, a proton is shifted towards the oxygen atom of methanol, but it is not completely transferred. Instead, a strong hydrogen bond is formed.

The Arrhenius diagram of the HHH transfer in the 2:1 complex is depicted in Fig. 6b. The kinetic isotope effects are similar to those expected for a single-barrier process according to Fig. 6a. They exhibit little dependence on temperature, indicating a rather narrow barrier. Unfortunately, the reacting complex could not be observed directly, allowing its structure to be studied in more detail. Note, however, that this complex was proposed by Northrop[86] as a model for the catalytic sites of certain proteases.

The tautomerism of porphyrin: tunneling into an intermediate

In this section, we consider the tautomerism of porphyrin as example of tunneling into an intermediate state as a source of temperature-independent kinetic isotope effects. The general reaction scheme of a stepwise degenerate HH transfer is illustrated in Scheme 1. In each reaction step a single H is transferred. Neglecting secondary kinetic isotope effects, the

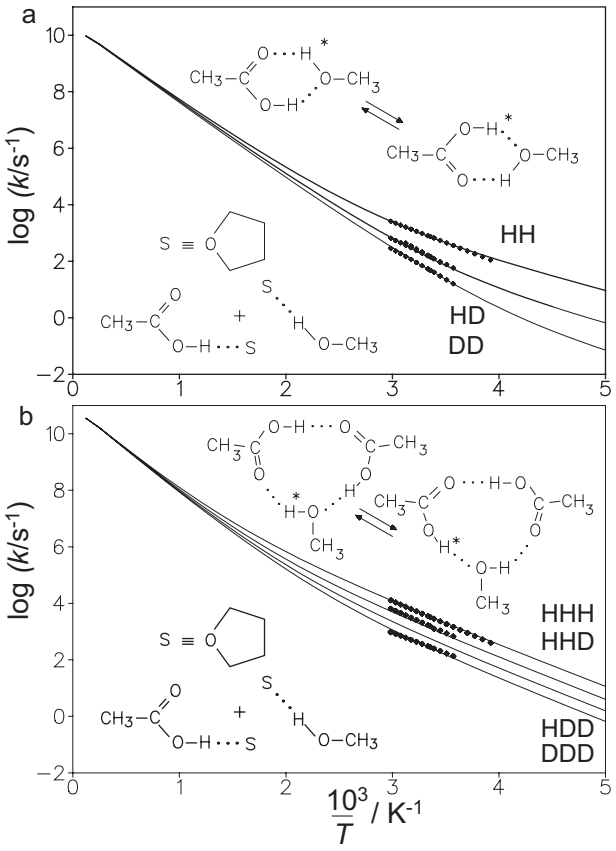

Figure 6. Arrhenius curves of the HH and HHH transfer between acetic acid and methanol in tetrahydrofuran. The data were taken from Gerritzen *et al.*[28,29] The solid lines were calculated using the parameters listed in Table 2

observed rate constants of the HH, HD, and the DD reaction are given by[87–91]

$$k^{HH} = k^{H},\ k^{HD} = \left[\frac{2k^{D}}{1 + k^{D}/k^{H}}\right],\ k^{DD} = k^{D} \qquad (7)$$

In fact, the three reactions are characterized by only two rate constants k^{H} and k^{D}, which represent the single H-transfer rate constants from the ground state into the intermediate states. In

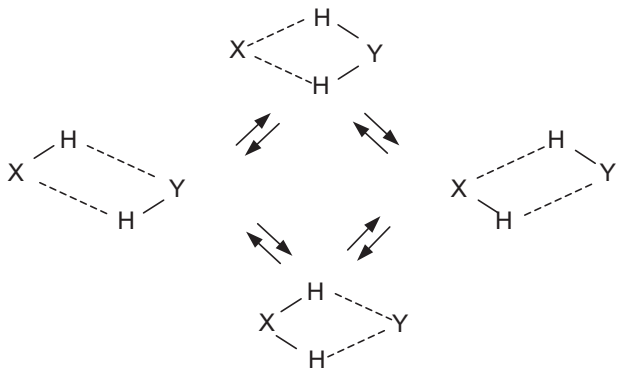

Scheme 1. Stepwise degenerate double proton transfer involving intermediates

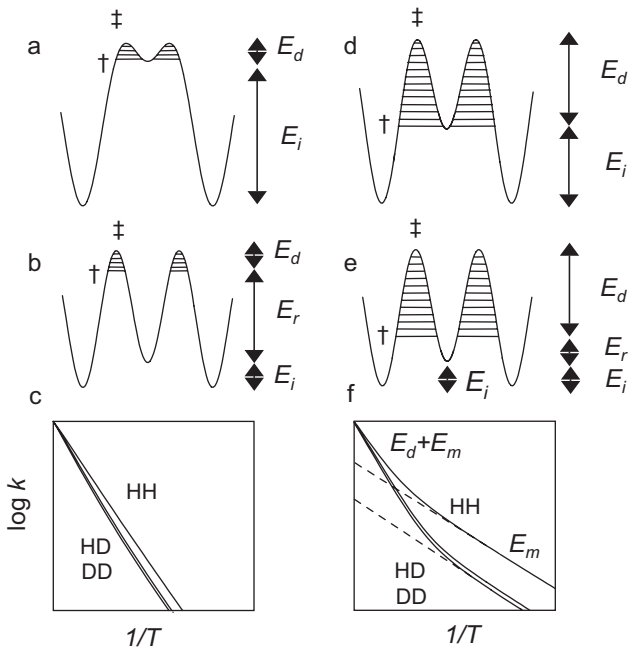

Figure 7. Schematic portrayal of a modified Bell tunneling model for degenerate, stepwise double proton transfers involving an intermediate. A minimum energy E_m is required for proton tunneling, which can take place only in the hatched regions. E_d is the height of the energy barrier above E_m. In parts (a) and (d), E_m is given by the energy of formation of the intermediate, E_i, from the reactants. In parts (b) and (e), E_m is given by $E_i + E_r$ where E_r is associated with heavy atom reorganization in the reactant state that necessarily precedes the proton transfer. Part (c) shows Arrhenius curves calculated in terms of the Bell–Limbach tunneling model for the circumstances in parts (a) and (b). Part (f) shows Arrhenius curves calculated in terms of the Bell–Limbach tunneling model for the circumstances in parts (d) and (e). Adapted from Reference [98]

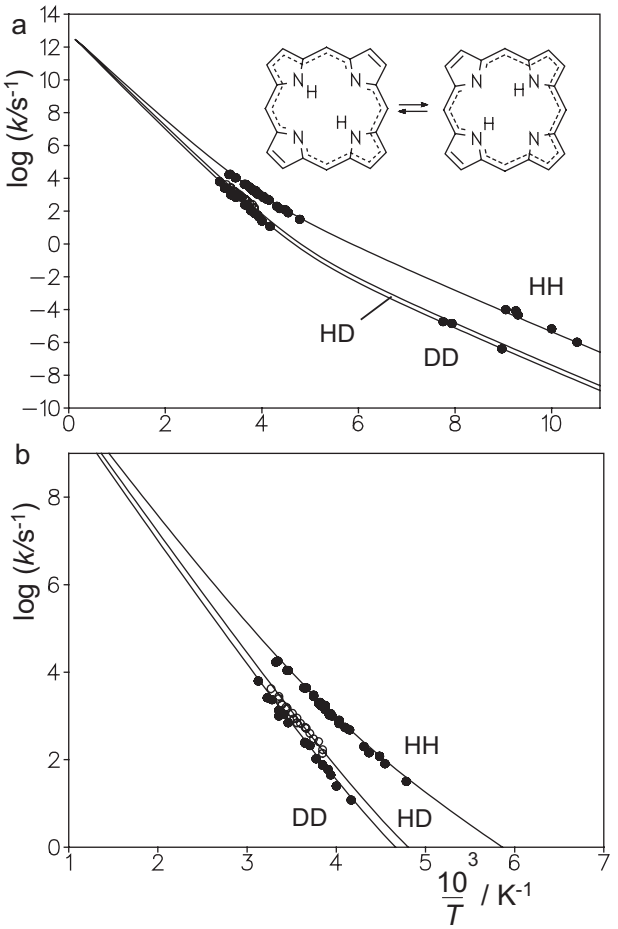

Figure 8. Arrhenius curves (calculated on the Bell–Limbach model) for the HH, HD, DD-transfer reactions of porphyrin. The measurements were made in liquid toluene-d_3, solid hexane, and in the porphyrin solid state and are combined in the Arrhenius plots. (a) Results for the entire temperature range. (b) Results for the high-temperature region only. Adapted from Reference [90]

cases where k^H/k^D is large, $k^{HD} = 2k^{DD} = 2k^D$. Thus, we only need to discuss the HH and DD Arrhenius curves.

Different situations are illustrated schematically in Fig. 7. In all cases, the total barrier heights $E_d + E_m$ for each single reaction step were assumed to be the same. In addition, it is assumed that the classical kinetic hydrogen/deuterium isotope effects for the over-barrier reactions are the same. Therefore, in the high-temperature regime, the associated Arrhenius curves coincide. However, drastic differences are expected at lower temperatures when tunneling becomes important. In this region, temperature-independent kinetic isotope effects are expected, leading to parallel Arrhenius curves. Tunneling can occur only at energies indicated by the hatched areas. In Figs 7a and 7d the minimum energy E_m for tunneling to occur is given by the energy of the intermediate E_i, whereas in Figs 7b and 7e an additional reorganization energy E_r is assumed, mainly used to compress the hydrogen bond as discussed in the theoretical section. This hydrogen bond compression may involve additional molecular conformational changes. The corresponding Arrhenius curves are depicted in Figs 7c and 7f. It is clear that it is not possible to determine the two contributions to E_m on the basis of the Arrhenius curves, as only one low-temperature slope can be measured experimentally. For that, one needs to study a series of related systems, where, for example, the reorganization energy is controlled by the chemical structure.

The first example known to us is the tautomerism of porphyrin. The determination of the kinetics by NMR[87–91] and optical methods[92] as well as the mechanism has been reviewed recently.[31] The full HH/HD/DD Arrhenius diagram[90] is illustrated in Fig. 8a, whereas Fig. 8b represents the high-temperature section alone. The fit of the experimental data to Eqn (7) is very satisfactory, where the solid lines were recalculated here using the Bell–Limbach model, with the parameters included in Table 2. This result also means that there is no substantial decrease of the zero-point energies of the two protons in the *cis*-intermediate states as compared to the initial and final *trans*-states, as this would increase the HD/DD isotope effect beyond the value of 2.

Before the full Arrhenius diagram is discussed in detail, let us first include the results of a subsequent study of Braun *et al.*[91] who measured the rate constants k^{HT} and k^{TT} using liquid-state ^{3}H NMR of tritiated porphyrin dissolved in toluene. In order to discuss the new data, it is convenient to convert the rate constants k^{LL} into the rate constants k^L using Eqn (7) which is naturally valid also for $L = T$. The resulting single H/D/T Arrhenius diagram of the porphyrin *trans–cis* reaction is depicted in Fig. 9.

Table 2. Bell–Limbach tunneling model parameters of various H-transfers

System	Reference	$k_{298\,K}/s^{-1}$	$KIE_{298\,K}$	E_m/ kJ mol^{-1}	ΔH/ kJ mol^{-1}	ΔS/ J K^{-1} mol^{-1}	*log* (A/s^{-1})	E_d/ kJ mol^{-1}	Δm/ amu	$2a$/Å	$\Delta\varepsilon$/kJ mol^{-1}
N, *N*′-diphenyl-6-aminofulvene-1-aldimine crystalline	[106]	3×10^{10}	9	2.1	—	—	12.6	10.2	1	0.66	5.2
N, *N*′-diphenyl-6-aminofulvene-1-aldimine amorphous	[106]	2×10^{11}	4	2.1	—	—	12.6	5.9	1.5	0.40	3.1
Porphyrin organic solvents/solid state	[90,91]	16 000	HH/DD 11.5 HH/HD 6.5 HD/DD 1.9 H/D 11.4 D/T 3.4 H/T 39	22.7	—	—	12.6	28.7	2.5	0.48	HD 4.9 DT 3.0
Porphyrin anion organic solvent/ solid phosphazene matrix	[94]	10^5	H/D 16.5 D/T 3 H/T 49.6	10.0	—	—	12.6	34.3	0	0.87	HD 6.5 DT 4.2
Azophenine in organic solvents	[95,100]	720	HH/HD 4.1 HD/DD 1.4	27.2	—	—	12.6	30.1	1.5	0.6	HD 3.8
Tetraphenyloxalamidine in CD_2Cl_2	[96]	1500	HH/HD 3	44.4	—	—	12.6	24	1.5	0.42	HD 2.5
Oxalamidine OA7 in methylcyclohexane	[97]	14	HH/HD 3.1 HD/DD 1.5	52.7	—	—	12.6	27.2	1.5	0.2	HD 2.9
Oxalamidine OA7 in acetonitrile	[97]	75	HH/HD 3.2 HD/DD 1.6	52.7	—	—	12.6	16.7	1.5	0.2	HD 3.8
Polycrystalline $^{15}N,^{15}N'$-di-(4-bromophenyl)-formamidine	[75]	1.3×10^7	HH/HD 5.6 HD/DD 4.1 HH/DD 23	9.2	—	—	12.4	24.7	1.5	0.44	HH/HD 2.9 HD/DD 2.9
2-hydroxyphenoxyl radical CCl_4 + dioxane	[82]	2×10^7	H/D 56	0.0	21	38	12.6	27.2	0	0.3	6.7
Di-tertbutyl-2-hydroxyphenoxyl radical in heptane	[80,81]	4×10^9	H/D 9.8	1.26	—	—	12.6	23.9	1	0.17	3.3
CH_3COOH+CH_3OH in THF	[28]	750	HH/HD 5.1 HD/DD 3.1 HH/DD15.5	16.5	16.5	−42	12.6 (10.4)	36	0	0.44	HH/HD 0.64 HD/DD 0.64

(*Continues*)

Table 2. (Continued)

System	Reference	$k_{298\,K}/s^{-1}$	$KIE_{298\,K}$	E_m/ kJ mol^{-1}	ΔH/ kJ mol^{-1}	ΔS/ J K^{-1} mol^{-1}	log (A/s^{-1})	E_d/ kJ mol^{-1}	Δm/ amu	2a/Å	$\Delta\varepsilon$/kJ mol^{-1}
2 CH_3COOH+CH_3OH in THF	[28]	3200	HHH/DDD 11.5 HHH/DHH 2.1	27.2	27.2	−34	12.6 (11)	33.5	0	0.2	0.25
Thermophilic Dehydrogenase *bs*ADH low temperature state 1	[30]	90	H/D *ca.* 5–8 (intrinsic)	41.8	—	—	12.6	48.1	0.5	0.36	5.86
Thermophilic Dehydrogenase *bs*ADH high temperature state 2	[30]	90	H/D 4.8 (intrinsic)	55.7	100[a]	333[a]	12.6	33.5	0	0.14	0.0
D-glucose dehydrogenase Ta-GDH low-temperature state 1	[119]	(1.3×10^4)[b]	H/D *ca.* 1.7–2.3	40	240[a]	786[a]	12.6	16.7	1	0.24	0.0
D-glucose dehydrogenase Ta-GDH high-temperature state 2	[119]	(1.3×10^4)[b]	H/D 2	32	—	—	12.6	24.7	4	0.2	0.0

[a] Enthalpy and entropy changes for the formation of state 2 (dominant at high temperatures) from state 1 (dominant at low temperatures). These values are so poorly determined by the data that the only conclusion merited is that both the enthalpy change and the entropy change are large and positive.
[b] Standard-state concentration of the β-anomer of D-glucose 1 M.

Figure 9. Arrhenius diagrams for the uphill *trans–cis* H/D/T-transfer reactions of porphyrin. Data and fits were measured and calculated analogously to those in Figure 8; liquid-state and solid-state data from Reference [91] are combined

This representation allows one to make a direct comparision with the Arrhenius diagram of the tautomerism of the deprotonated unsubstituted porphyrin anion depicted in Fig. 10. The tautomerism of the latter was discovered by Braun *et al.*,[93] and the rate constants k^H were measured for the liquid and the solid state, as well as k^D and k^T for the liquid state.[94] Whereas the reaction profile for the anion is symmetric, it is asymmetric for the parent compound as illustrated schematically in Fig. 11.

For the parent compound porphyrin, an Arrhenius curve pattern of the type discussed in Fig. 1b is observed. Noteworthy is the same low-temperature slope E_m of the Arrhenius curves of the HH and DD reaction in Fig. 8, i.e., of the H- and D-reaction in Fig. 9. E_m will be caused mainly by the asymmetry of the reaction profile because at least the energy of the *cis*-intermediate is required for tunneling to occur, but the reorganization energy of the ring skeleton will also contribute. Also note that the low-temperature kinetic H/D isotope effect is smaller than predicted from the relatively large barrier difference for H and D evaluated at high temperatures. In order to match this effect, a relatively high value of Δm for the heavy-atom tunneling contribution had to be used in order to reduce the low-temperature isotope effect.

By contrast, this was not necessary in the case of the porphyrin anion where the transfer is degenerate and where the

Journal of Physical Organic Chemistry

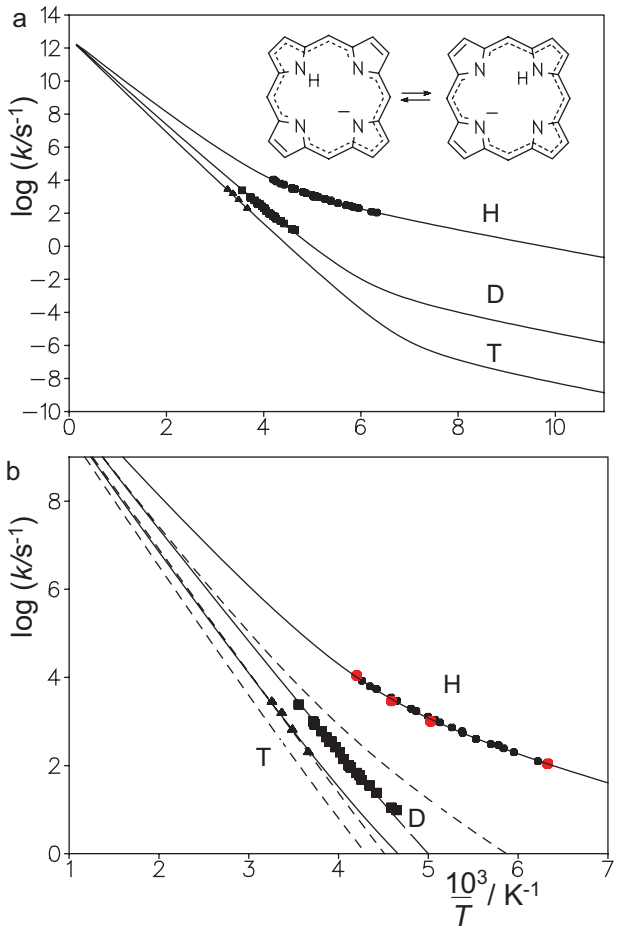

Figure 10. Arrhenius diagrams for the tautomeric H/D/T-transfer reactions of porphyrin anion. Data and fits were measured and calculated analogously to those in Fig. 8; liquid-state and solid-state data from Reference [94] are combined. The dashed lines represent the Arrhenius curves of the parent compound from Fig. 9b

low-temperature kinetic isotope effects are substantially larger than in the parent compound. Therefore, the much smaller value of E_m in the anion is assigned to the reorganization of the porphyrin skeleton preceding the transfer. Both the tunneling distances and the isotopic differences in barrier heights are larger than for the parent compound. These findings can be associated with the symmetry of the potential curve in the anion.

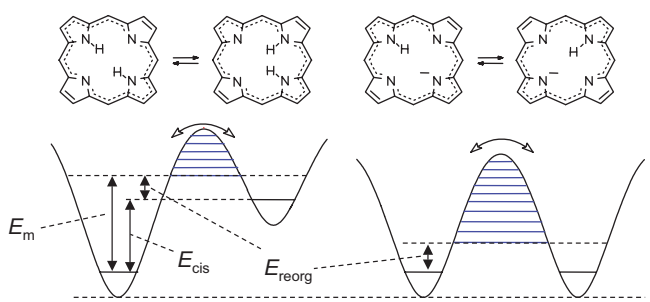

Figure 11. Schematic potential curves for the tautomerism of porphyrin and its mono-deprotonated anion. Adapted from Reference [91].

Molecular structure and hydrogen bond compression in intra- and intermolecular hydrogen transfers

The intramolecular degenerate double proton transfers of azophenine (AP)[95] and of oxalamidine (OA) derivatives (Scheme 2)[96–99] represent interesting cases which demonstrate the importance of the molecular structure on how hydrogen bond compression leading to the pre-tunneling state assists the hydrogen transfer. These systems have been studied by dynamic NMR spectroscopy of the ^{15}N labeled compounds. However, processes could neither be detected in the case of solid BIM, nor in the bicyclic oxalamidines OA5 and OA6 dissolved in organic solvents. TPOA exhibited a mixture of various slow exchanging conformers where only the conformer exhibiting two weak intramolecular hydrogen bonds was subject to a degenerate intramolecular double proton transfer for which rate constants of the HH and of the HD reaction could be measured. Full kinetic HH/HD/DD isotope effects could be measured only in the case of AP and OA7.

The Arrhenius diagrams are depicted in Fig. 12. In all cases, the reactions in solution were suppressed in the solid state indicating major heavy-atom motions in addition to H-bond compression.

The kinetic HH/HD/DD isotope effects satisf ied Eqn (7) well and were hence typical for stepwise degenerate reaction mechanisms involving metastable *cis*-intermediates reached by single H transfers as illustrated by Scheme 1. In a similar case as described above for porphyrin, the observed rate constants k^{LL} could be converted into the rate constants k^{L} of the uphill single H transfers. k^{H} and k^{D} were then calculated in terms of the Bell–Limbach tunneling model using the parameters included in Table 2 and converted back to k^{LL} using Eqn (7).

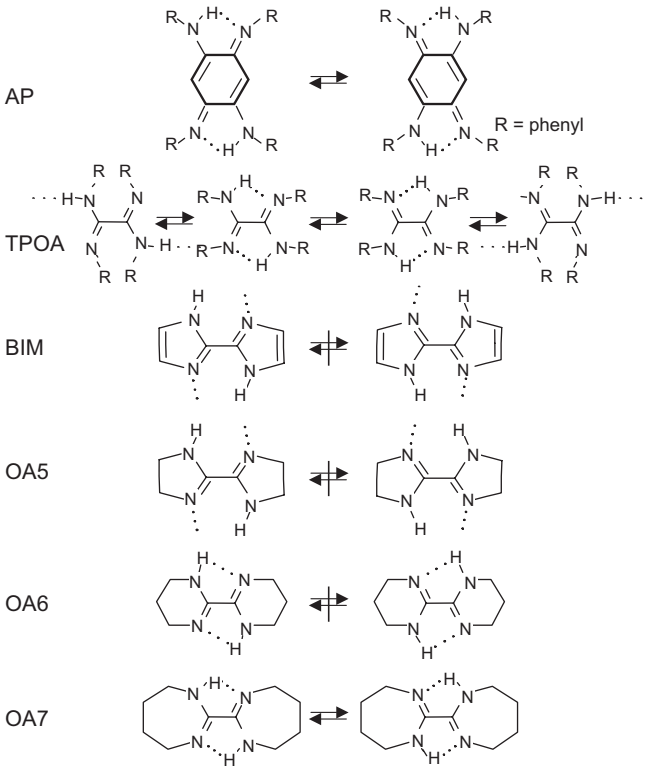

Scheme 2. Intramolecular double proton transfers in azophenine (AP)[95,100] and oxalamidine (OA) derivatives[96–99] TPOA: tetraphenyloxalamidine; BIM: bisimidazolyl; OA5: 2,2′-bis(4,5-dihydro-l,3-diazole); OA6: 2,2′-bis-(3,4,5,6-tetrahydro-1,3-diazixine). OA7: 2,2′-bis-(4,5,6,7-tetrahydro-1,3 diazepine)

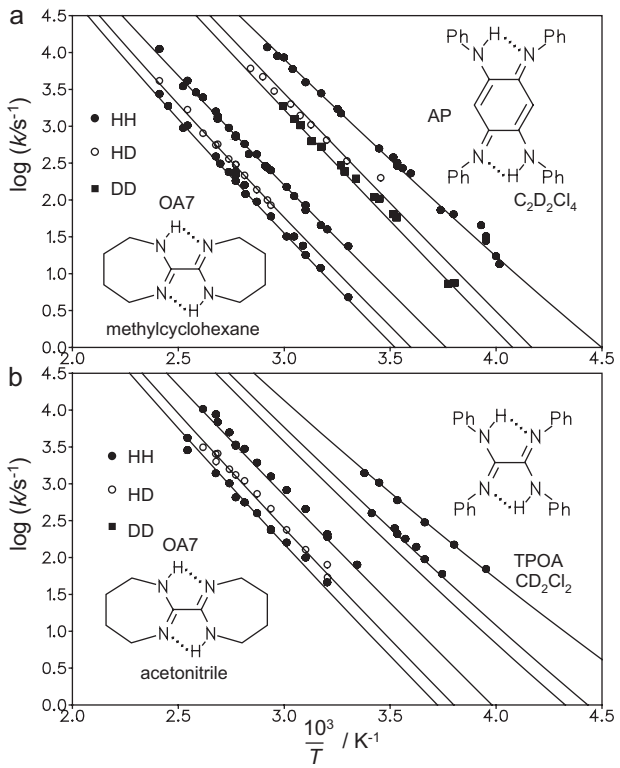

Figure 12. (a) Arrhenius diagrams for the tautomerism of azophenine[95] (AP) in $C_2D_2Cl_4$ (top) and of the seven-membered bicyclic oxalamidine OA7 in methylcyclohexane[97,98] (bottom). (b) Arrhenius diagrams for the tautomerism of tetraphenyloxalamidine (TPOA) in CD_2Cl_2 (top[97]) and of OA7 in acetonitrile (bottom[97,98]). The solid lines were calculated on the Bell–Limbach model using the parameters listed in Table 2 as described in the text

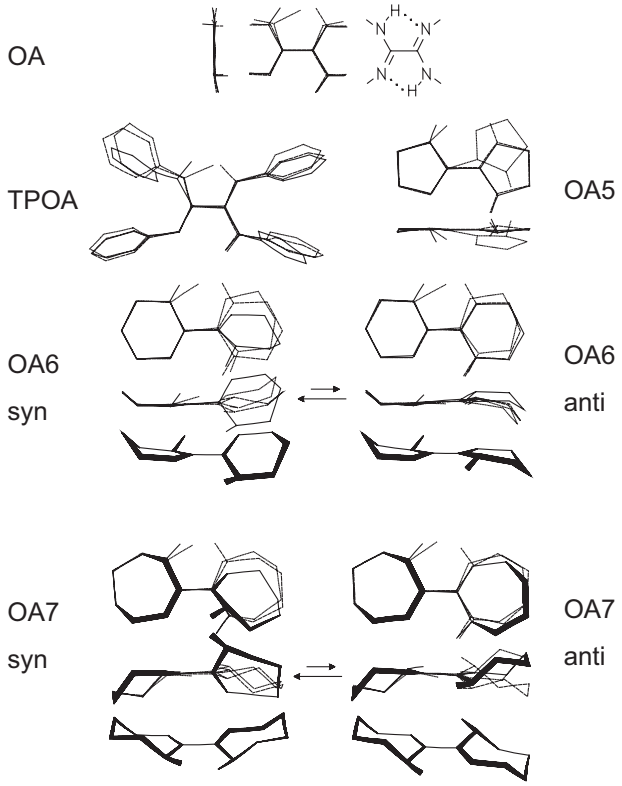

Figure 13. Heavy atom reorganization during HH transfer in oxalamidines calculated using the semiempirical PM3-MNDO method. Adapted from Reference [99]

The reaction rates of tetraphenyloxalamidine (TPOA) dissolved in CD_2Cl_2 are only slightly larger than those of azophenine (AP) dissolved in $C_2D_2Cl_4$. The kinetic isotope effects are larger in the latter; moreover, they depend on temperature, whereas those of TPOA exhibit little temperature dependence. The tautomerism of the bicyclic oxalamidine OA7 is, on the other hand, substantially slower than of TPOA. In the corresponding six-membered bicyclic oxalamidine OA6 no double proton transfer was detectable.[98] On the other hand, the tautomerism of OA7 was substantially faster in acetonitrile (dielectric constant 37.5) as compared to methylcyclohexane (dielectric constant 2.02) as illustrated in Fig. 12. These findings supported the formation of a zwitterionic intermediate according to the stepwise mechanism of Scheme 1. The small dependence of the kinetic isotope effects of temperature is confirmed for OA7 as the Arrhenius curves of the isotopic reactions are almost parallel. Note that a quantitative discussion of these parameters is difficult as the temperature range of the experimental data was limited. Therefore, the parameter sets obtained are not unique.

However, qualitatively the above findings and the tunnel parameters obtained can be explained in terms of Fig. 7 by a combination of a reorganization energy E_r and an intermediate energy E_i which determine E_m. The large changes in the experimental activation energies in the tautomerism of the oxalamidines and of azophenine, and at the same time the small changes of the kinetic isotope effects indicate then that the main differences arise from different values of $E_m = E_r + E_i$. It is plausible that the changes within the oxalamidines are then mainly given by different reorganization energies E_r.

This hypothesis was confirmed by semi-empirical calculations for various oxalamidines.[99] The results are visualized in Fig. 13. In all cases, a substantial heavy-atom reorganization precedes the H-transfer which is strongly dependent on the chemical structure. This reorganization mainly involves a decrease of the nitrogen–nitrogen distances of the hydrogen bond in which the proton transfer takes place, thus lowering the barrier for the tautomerism. Thus, in all other cases, H-bond compression is associated with major conformational changes, requiring an additional reorganization energy. In TPOA and azophenine (not shown), H-bond compression is associated with a phenyl group reorientation. This reorganization is not possible in the solid state, where only single tautomers are formed[98,100] The bicyclic oxalamidines also require a ring reorganization for H-bond compression to occur, which is smaller for OA7 as compared to OA5 and OA6, in accordance with experimental findings. For OA6 and OA7 *syn*- and *anti*-conformations were found, which both exhibited similar energies for the transition states.

In all cases, the molecular structures do not allow for a simultaneous compression of both hydrogen bonds, something which would require a very high energy. Therefore, the transfers are stepwise as indicated by Scheme 1.

The effects of small changes in molecular structure can be observed in the case of the related diarylamidines[101–103] which are the nitrogen analogs of formic acid and which represent models for nucleic acids. The tautomerism of polycrystalline $^{15}N,^{15}N'$-di-(4-bromophenyl)-formamidine (DBrFA) has been

Journal of Physical Organic Chemistry

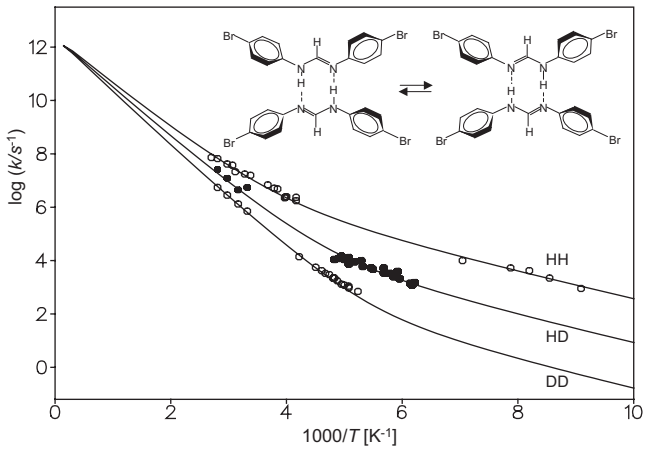

Figure 14. Arrhenius diagrams for the degenerate HH, HD and DD transfer in cyclic dimers of polycrystalline $^{15}N,^{15}N'$-di-(4-bromophenyl)-formamidine (DBrFA). Adapted from Reference [75]

studied by dynamic solid state NMR[104,105] leading to the full Arrhenius diagram of Fig. 14.[75] Two large HH/HD and HD/DD isotope effects have been observed, indicating a single barrier process for the transfer of both hydrons. At low temperatures, evidence for a process leading from the ground state to the pre-tunneling state was again observed. By comparison with other formamidines, the reaction scheme illustrated in Fig. 15 was postulated which shows how aryl group reorientation and hydrogen bond compression interfere with each other.

For that reason, symmetric diarylamidines with varying substituents in *p*-position of the phenyl rings were studied by X-ray crystallography and dynamic solid state ^{15}N NMR.[104,105] The tendency to form cyclic dimers in the solid state was supported. In most of the cases, the angles α_N and α_{NH} between the phenyl groups and the molecular skeleton at the imino and the amino nitrogen atoms were different for a given molecule; the aryl ring at the amino nitrogen atom was often found to be coplanar to the molecular skeleton, but a substantial angle was observed at the amino nitrogen. This circumstance can be attributed to steric interactions of aromatic o-CH groups and the CH group of the amidine unit. It leads to a large preference for one of the two potentially degenerate tautomers, and suppresses the HH reaction in the solid. A degenerate HH transfer was observed only in the OCH_3 substituted compound, where the two angles were similar but not coplanar with the molecular skeleton.

In solution the aryl groups of a cyclic dimer will, therefore, not be the same, leading to an asymmetry of the double well for the HH transfer as illustrated in Fig. 15. Reorientation of the phenyl groups to angles around 50° will symmetrize the potential and minimize the barrier height of the HH transfer. The latter is expected to take place in this configuration. Finally, the process is completed by a reorientation of the aryl groups. This means that the total barrier of the HH reaction in solution within the cyclic dimer will be slightly higher than in the symmetric configuration in the solid state. This is indeed what was observed for the rate

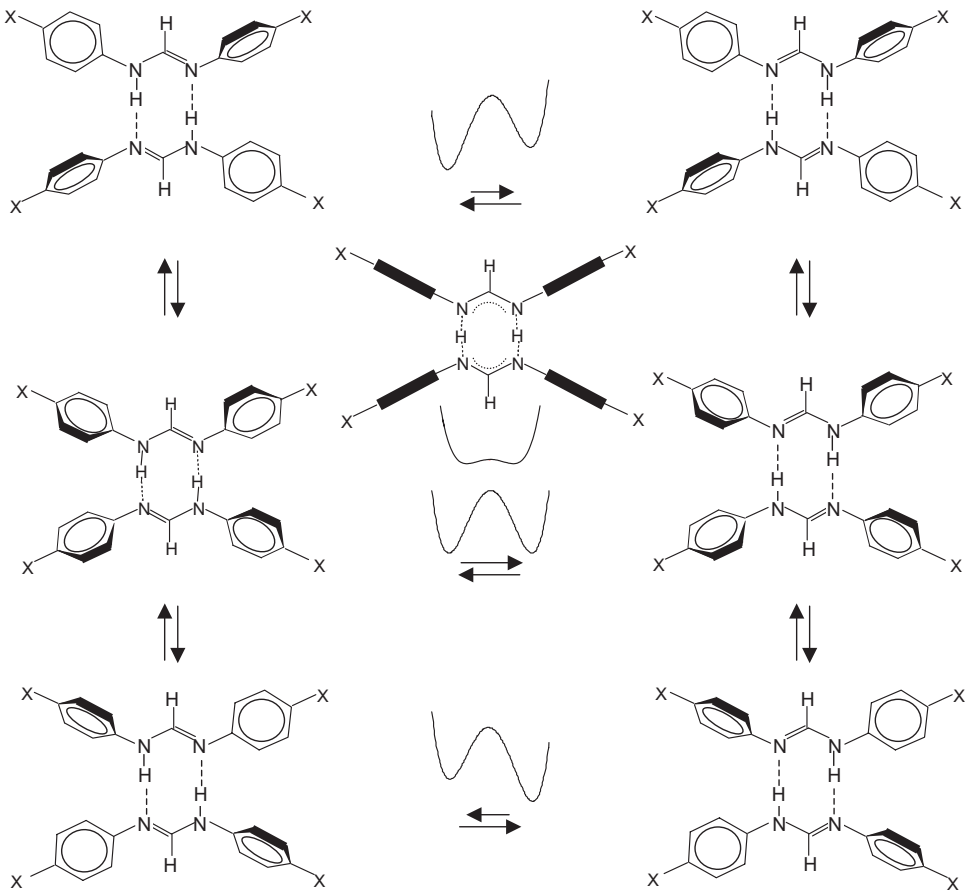

Figure 15. Aryl group torsion, hydrogen bonding, and double proton transfer in diarylformamidines. One-dimensional schematic potential curves for the double proton transfer are included. Adapted from Reference [75]

constants of the OCH_3-substituted diarylamidine in the solid state.

Finally, we discuss in this section a recent example of the tautomerism of solid *N*, *N*′-diphenyl-6-aminofulvene-1-aldimine (PALDIM). The process observed[106] takes place in the nano- to picosecond timescale and represents to our knowledge the fastest single H transfer reaction where rate constants have been measured by NMR including kinetic H/D isotope effects. Two modifications were observed in the solid state: an amorphous and a crystalline form. The Arrhenius curve of the amorphous form is depicted in Fig. 16. It represents an excellent example of the theoretical Arrhenius curve of Fig. 1b: (i) temperature-independent kinetic isotope effects are observed at low temperatures leading to parallel Arrhenius curves for the H and the D reactions; (ii) temperature-dependent kinetic isotope effects are observed at high temperatures according to a reaction over the barrier. The reaction is much slower in the crystalline state (Fig. 17). These features can be explained in terms of a coupling of the *N*.*N* distance and hence the barrier to phenyl group reorganization similar to the case of the diarylamidine dimer. In the amorphous state this reorganization might involve less energy than in the polycrystalline state.

The relation between hydrogen bond geometries, hydrogen bond compression, and barriers for H transfer between nitrogen atoms has been discussed recently for several systems exhibiting intramolecular NHN hydrogen bonds.[106] Figure 18a depicts the NHN hydrogen bond correlations according to the graph of Fig. 2. The dotted line was estimated using an empirical correction for quantum zero-point vibrations of the H-bonded proton and is assumed to be better able to reproduce experimental geometries as compared to the solid line.[76,77] The geometry of crystalline PALDIM (**Ic**) was estimated from the crystallographic *N*..*N* distance and *ab initio* calculations.[107,108] The geometry of tetramethyldibenzotetraaza[14]annulene (**II**)[109,110] was derived from the X-ray crystal structure and dipolar ND couplings. The geometries of the porphyrin anion (**III**) and of the transition state **III**‡ of H transfer were taken from *ab initio* calculations.[111,112] The graph suggests that H transfer involves two stages. In the first stage, hydrogen compression takes place preferentially along the

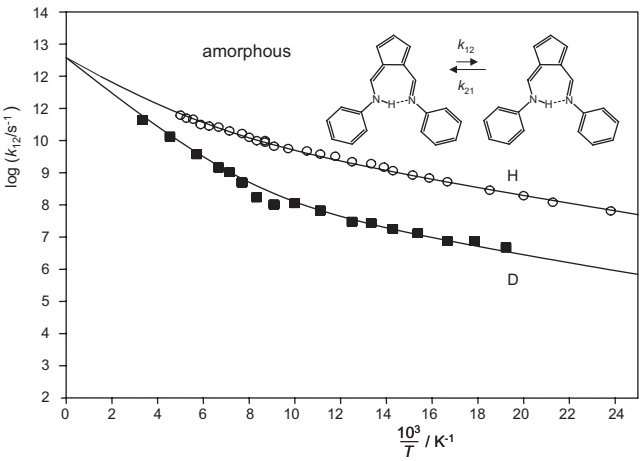

Figure 16. Arrhenius diagram for the solid state tautomerism of amorphous isotopically labeled *N*,*N*′-diphenyl-6-aminofulvene-1-aldimine (PALDIM). The solid lines were obtained by fitting the experimental data using the Bell–Limbach tunneling model with the parameters of Table 2. Adapted from Reference [106]

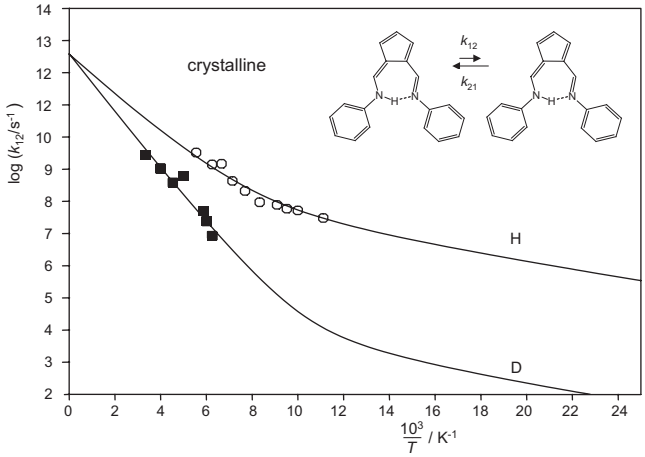

Figure 17. Arrhenius diagram for the solid state tautomerism of polycrystalline isotopically labeled PALDIM. The solid lines were obtained by fitting the experimental data using the Bell–Limbach tunneling model with the parameters of Table 2. Adapted from Reference [106]

correlation line until the pre-tunneling configuration is reached where H is transferred at a given value of q_2 from the left to the right side of the correlation curve, going through the transition state at $q_1 = 0$. Here, tunneling and zero-point energy changes along the minimum energy pathway will dominate the overall kinetic H/D isotope effects. We note that evidence for such a two-stage process has been found in *ab initio* calculations of porphyrin.[113]

Figure 18b plots the total barrier $E_m + E_d$ and of E_m obtained by analyses of the Arrhenius curves of the corresponding H transfers (Table 2) as a function of the hydrogen bond distance q_2. For the systems considered, E_m represents the reorganization energy to reach the pre-tunneling state. It is shown that these energies increase strongly with the q_2 value of the reactant state. It is astonishing that the reorganization energy E_m represents about 20% of the total barrier energy $E_m + E_d$. Because of the excellent correlation we placed the experimental values of $E_m + E_d$ and of E_m of amorphous PALDIM (**Ia**) on the dotted lines (open symbols), from which we estimate that the hydrogen bond in this phase is somewhat stronger than in the crystalline form (Table 2), as represented by the open symbols in Fig. 18a. Thus, as compared to the crystalline form, the smaller barrier and reorganization energy and the smaller kinetic H/D isotope effects of the amorphous form of **I** are interpreted in terms of a stronger NHN hydrogen bond.

Large temperature-independent kinetic isotope effects in H transfer from carbon centers in enzymes

Klinman *et al.*,[37,113–118] Sutcliffe *et al.*,[32] and others have observed temperature-independent kinetic isotope effects for H transfer in a number of enzyme reactions. Arguments similar to those of the present paper allow these results also to be explained in terms of heavy-atom motions preceding the actual H transfer. These studies are covered elsewhere in this symposium in print. We comment here on only two examples, which involve a molecular transition between two tunneling regimes.

A thermophilic alcohol dehydrogenase from *Bacillus stearothermophilus* (*bs*ADH) was studied by Kohen *et al.*[119] and a D-glucose dehydrogenase from the archaeon *Thermoplasma acidophilum* (Ta-GDH) was studied by Anandarajah *et al.*[120] Both

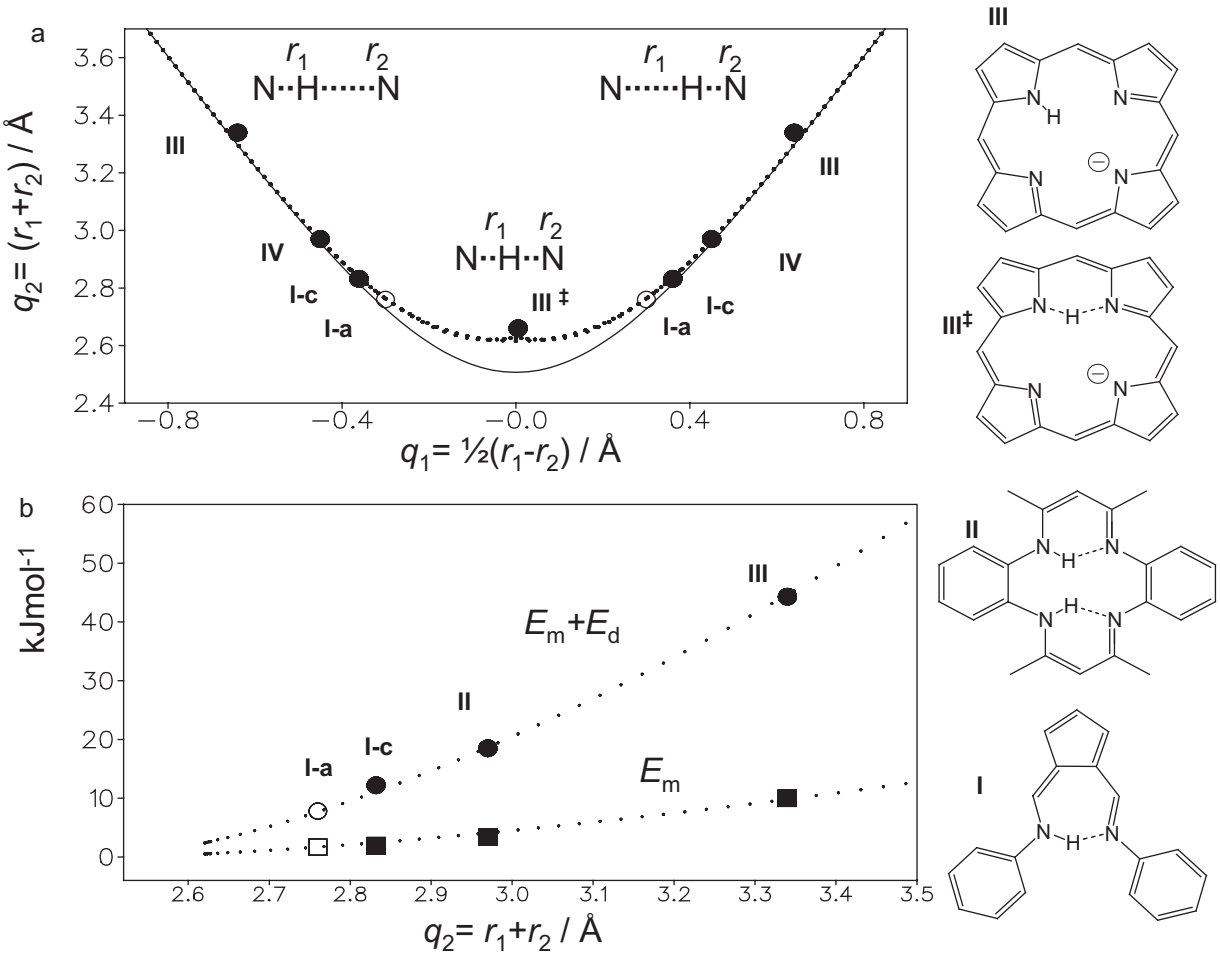

Figure 18. (a) Hydrogen bond geometries of various molecular systems containing NHN hydrogen bonds. (b) Total barrier height $E_d + E_m$ and minimum energy for tunneling E_m of the H transfers calculated from the Arrhenius curves of the species in (a) (refer Table 2 and text). Adapted from Reference [106]

enzymes catalyze the transfer of a hydride ion between a carbon center of the substrate and nicotinamide adenine dinucleotide (NAD^+) as depicted schematically in Fig. 19. The Arrhenius diagrams are depicted in Fig. 19a, and the kinetic H/D isotope effects in Fig. 19b.

In the case of *bs*ADH, a sudden change of the apparent slope and of the intercept of the Arrhenius curves for the H and D reactions is observed around room temperature. An initially puzzling feature is that the KIEs are independent of temperature in the high-temperature regime but dependent on temperature in the low-temperature regime.

The solid lines in Fig. 19a were calculated assuming the simple reaction network of Scheme 3. It is assumed that the enzyme adopts two different states 1 and 2 at equilibrium (K), where 1 is less reactive than 2 (Scheme 3). In the less reactive state 1 dominating at lower temperatures, the rate constant of H transfer is given by k_1, but in the more reactive state 2 dominating at higher temperatures by k_2. Assuming again that the H-transfer is slower than the conversions between the states we obtain the following expression by modification of Eqn (1),

$$k = x_1 k_1 + x_2 k_2 = k_1 \frac{1}{1+K} + k_2 \frac{K}{1+K} \qquad (8)$$

where x_1 and x_2 correspond to the mole fractions of states 1 and 2 and K is again the equilibrium constant for the formation of state 2 from state 1. According to Table 2, state 2 dominates at higher temperatures in spite of its higher energy because its very large positive entropy. This state could be a state where the protein has become ideally flexible for proper activity, in contrast to the low-temperature regime. This conclusion is in accordance with the fact that this *bs*ADH was evolved to function at ~65 °C and with qualitative suggestions proposed in the past to rationalize the curved Arrhenius plot (Kohen *et al.*,[119] Kohen *et al.*,[121,122] Liang *et al.*[123]).

The tunnel parameters included in Table 2 are consistent with a ground-state tunneling mechanism in both temperature regimes, with temperature-independent kinetic isotope effects in both cases. The apparent temperature dependence at low temperatures is then the result of the transition between the two regimes, but does not arise from intrinsic temperature-dependent kinetic isotope effects. We note that in both states, the pre-exponential factor of $10^{12.6}\,s^{-1}$ employed throughout this study is consistent with the data. The minimum energy for tunneling to occur is larger in the high-temperature state 2, but the barrier height and the barrier width are smaller than for the low temperature state 1. Thus, there seems to be a substantial change of the barrier parameters coincident with the increased mobility of the enzyme at higher temperatures.

This interpretation is corroborated by the findings for Ta-GDH. The data for this reaction are for $k_{cat}/K_{M\beta}$ (a rate constant that

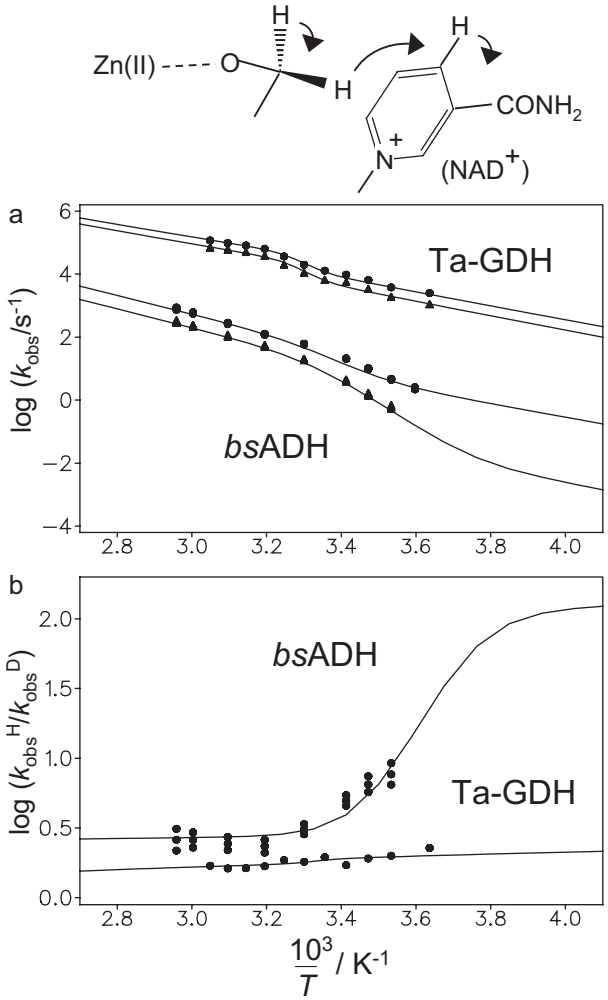

Figure 19. (a) Arrhenius curves for the isotopic H-transfer reactions in the action of a thermophilic alcohol dehydrogenase[30] of *Bacillus stearothermophilus* (*bs*ADH; $k_o = k_{cat}$) and in the action of a thermophilic D-glucose dehydrogenase of the archaeon *Thermoplasma acidophilum* (Ta-GDH; $k_o = k_{cat}/K_{M\beta}$ at a standard-state concentration of the β-anomer of D-glucose of 1 M). The kinetic data for *bs*ADH are taken from Kohen *et al.*[119] and those for Ta-GDH from Anandarajah *et al.*[120] (b) Temperature dependences of the kinetic H/D isotope effects. The isotope effects for *bs*ADH are intrinsic isotope effects, i.e., they refer only to the H-transfer step. The isotope effects for Ta-GDH are measured values and it is unknown whether they are intrinsic effects. The solid lines were calculated using the reaction network of Scheme 3 and the parameters listed in Table 2

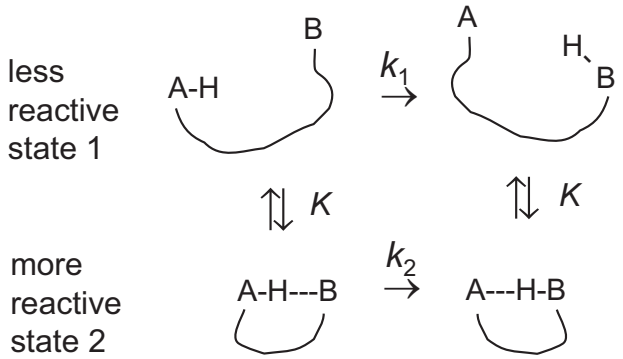

Scheme 3. Conformationally dependent H transfer in a biomolecule

incorporates the binding step for the reactive β-anomer of the substrate D-glucose) and the kinetic H/D isotope effects are apparently smaller than for the *bs*ADH reaction. The isotope effects are simply those observed and not necessarily the intrinsic effects. Again, at high temperatures temperature-independent kinetic isotope effects are observed, and at 310 K a transition to a second state occurs. The KIEs were found again to be temperature-independent according to the Bell–Limbach fit, as was postulated just above for the *bs*ADH reaction. The KIEs were around 2 in the high-temperature region and experimentally varied from 2.3 to 1.7 in the low-temperature region. As above, the latter variation can be attributed on the present model to the influence of the structural transition.

There are other matters to be noted about the comparison between the results for *bs*ADH and for Ta-GDH. Some of these features illustrate the advantages of using the Bell–Limbach model for examination of experimental data before launching major theoretical studies.

The rate constants for which data were obtained on *bs*ADH were k_{cat} values (dimensions s^{-1}) and, second, Kohen *et al.*[119] were careful to obtain the so-called *intrinsic isotope effects* at each temperature, i.e., the isotope effects for the H-transfer step alone, unaffected by other steps. These features are ideal for theoretical treatments of any kind and that fact is reflected in the results, particularly in the values of Δm; this quantity in the simplest sense represents the mass increment added by participation of non-hydrogen atoms in the tunneling event. The findings were values of 0.5 amu in the high-temperature region and zero in the low-temperature range. These seem quite reasonable suggesting that one reason for the quite modest KIE of about 5 at high temperatures is the participation of other atoms in the tunneling motion, a feature which is lost in the lower-temperature range, the KIEs then rising toward 8.

In contrast, the data for Ta-GDH consist of values of the rate constant $k_{cat}/K_{M\beta}$, the second-order rate constant (dimensions $M^{-1}s^{-1}$) for catalytic conversion of the β-anomer of D-glucose to product. The plots for Ta-GDH in Fig. 19a thus presuppose the choice of the standard-state concentration for the β-anomer of glucose to be 1 M, which converts k_{obs} to a first-order rate constant of appropriate dimensions. The chosen standard-state concentration cancels out of the isotope effects so that the plot for Ta-GDH in Fig. 19b requires no consideration of this matter. Also, as mentioned above, the data for Ta-GDH have not been examined[120] to determine whether the H-transfer event is fully rate-limiting and thus whether the measurements have produced intrinsic isotope effects or not.

Indeed the parameters emerging from the Bell–Limbach treatment (Table 2) are very informative about this last question. For the data in the low-temperature regime, the results are unremarkable. In particular the value of Δm is 1, suggesting some participation of non-hydrogen atoms in the tunneling event but nothing extraordinary. For the high-temperature regime, in contrast, a value of 4 is calculated which is so large as to appear unphysical. It is also an experimental fact that the KIEs in both regimes are only around 2. If the data correspond to intrinsic isotope effects, then some considerable participation of heavy atoms in the tunneling event might be required to bring the isotope effects down to 2. But if the effects are not intrinsic, and

Journal of Physical Organic Chemistry

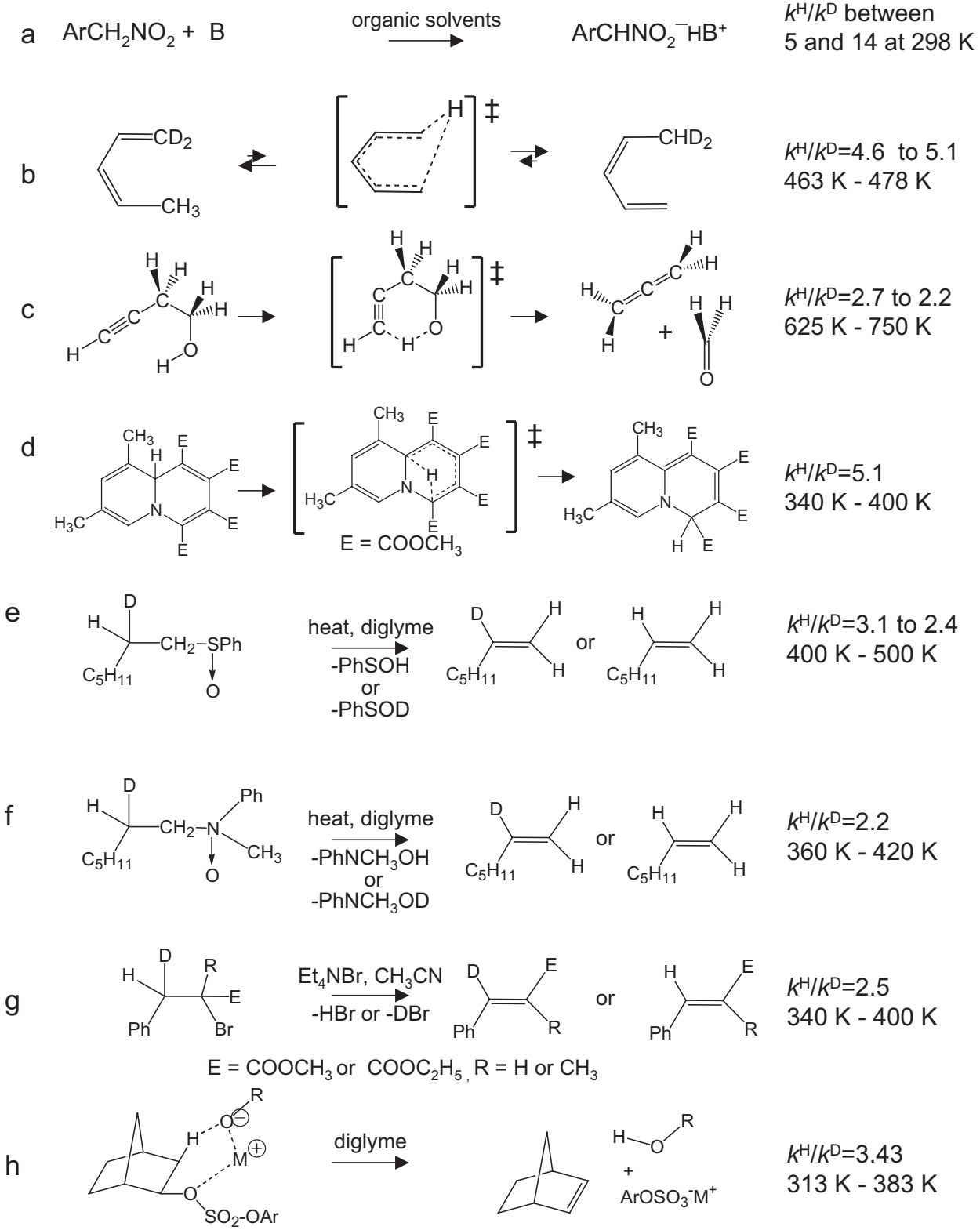

Scheme 4. Examples of hydrogen transfers from carbon centers in small organic molecules for which kinetic isotope effects have been determined. (a) Proton tranfer to strong nitrogen bases[124–130] (b) 1,5 sigmatropic hydrogen shift in pentadiene[131] and (c) in 3-butyn-1-ol[132] (d) Rearrangement of 9a*H*-quinolizine to 4*H*-quinolizine[137] (e) Sulfoxide and (f) aminoxide thermolysis[133] (g) β-elimination of α-bromoesters[134,135] (h) Ion-pair base-promoted syn-elimination of bicyclo[2.2.1] heptan-2-em-yl-toluene-*p*-sulphonate.[136]

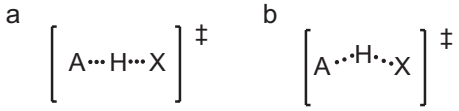

Scheme 5. (a) Linear *versus* (b) nonlinear transition state of H transfer from a heavy atom A to a heavy atom X

the intrinsic isotope effects are, as expected, larger than the observed effects, then the Bell–Limbach approach (which contains no provision for multiple rate-limiting steps) will be forced to reduce the predicted values to 2 by a fallaciously large value of Δm. Indeed, it seems likely that the large calculated value $\Delta m = 4$ reflects such an error. It would therefore be perilous for detailed theoretical work to be initiated before the data have been corrected to the intrinsic effects or at least tested to be sure whether or not they are intrinsic effects. In addition, it should be noted that the apparent thermodynamics of the state-to-state conversion (Table 2) specify large and positive values for both the entropy and enthalpy of conversion from state 1 to state 2. These values are determined by only a very few experimental points and thus their numerical values are highly uncertain; it is probably true that the values are both rather large and of positive sign but more cannot be said.

Temperature-independent kinetic isotope effects in small-molecule hydrogen transfers from carbon

In this section, we address the problem of kinetic isotope effects and tunneling in H abstractions from carbon. As CH-units cannot form strong hydrogen bonds with proton acceptors, H transfer takes place at larger heavy-atom distances than in the case of the more electronegative atoms such as nitrogen, oxygen, or fluorine. As a consequence, barriers for H transfer from carbon are substantially larger than in the case of the other heavy atoms.

The smallest barriers are found for cases of acidic CH groups and strong bases. For example, Caldin *et al.*[124–126] found that the abstraction of a proton from (4-nitropheny1) nitromethane by strong bases in polar and apolar solvents (Scheme 4a) generated unusually large isotope effects (initially thought to be around 40 (H/D) but later shown[127–130] to be of the order of 5–14). These latter values are still large enough to be consistent with the presence of tunneling. However, the isotope effects were dependent on temperature in the manner predicted by the original Bell theory, with $A_D > A_H$. This was also true for intramolecular sigmatropic 1,5-hydrogen shifts between two carbon atoms in pentadiene (Scheme 4b; König *et al.*[131]) and for H-shifts from carbon to oxygen (Scheme 4c; Kwart *et al.*[132]).

A surprise, therefore, was the discovery of temperature-independent primary KIEs (H/D) for H-transfer reactions in small organic molecules by Kwart *et al.*[133–138] Such a finding implies parallel Arrhenius curves for k^H and k^D with large values (essentially equal to the isotope effect) of the pre-exponential factor ratios A^H/A^D. In this work the isotope effects were determined in competitive experiments and so values of the individual isotopic rate constants k^H and k^D were not obtained. One example is the rearrangement of 9a*H*-quinolizine to 4*H*-quinolizine depicted in Scheme 4d.[137] Whereas the KIEs of the aminolysis reaction depicted in Scheme 4f were temperature independent, the isotope effects emerged as temperature dependent in the sulfoxide case[133] of Scheme 4e. Other temperature-independent KIEs were found for the β-elimination of α-bromoesters (Scheme 4g)[134,135] and for the ion-pair base-promoted *syn*-elimination of bicyclo[2.2.1] heptan-2-em-yl-toluene-

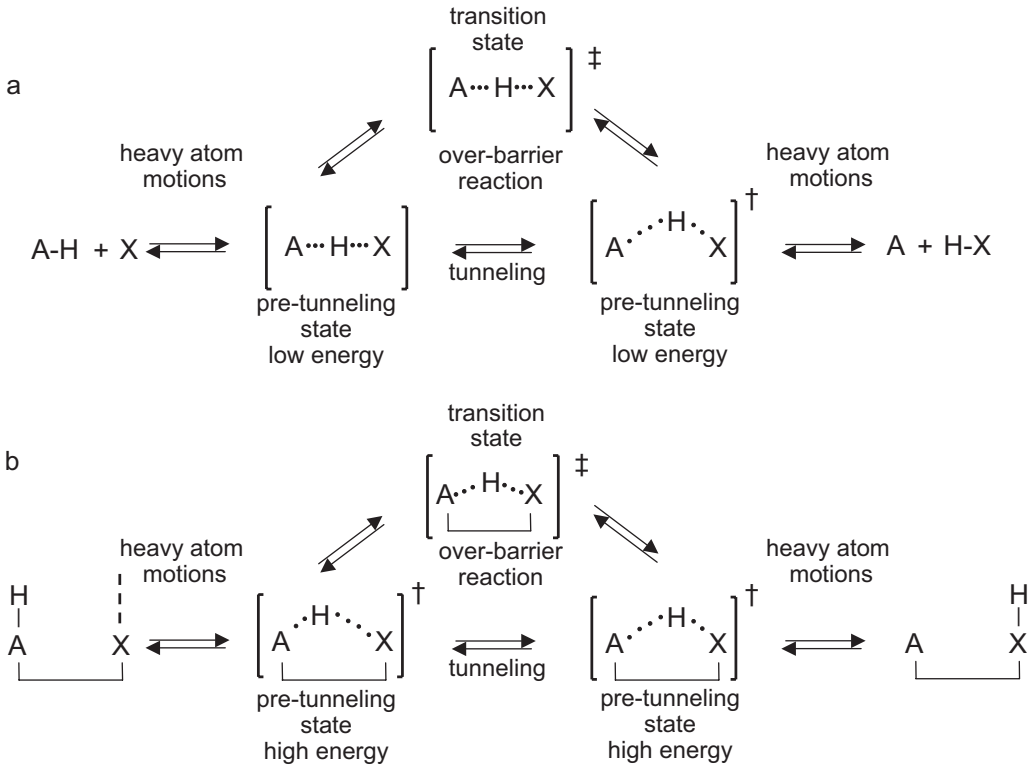

Scheme 6. General scheme proposed for hydrogen abstraction from a heavy atom A to a heavy atom X in intermolecular reactions (a) and intramolecular reactions (b)

p-sulphonate (Scheme 4h).[136] As mentioned above, absolute values of k^H and of k^D were rarely obtained and then over narrow temperature ranges.

At the time of the work just described, the prevailing view was that tunneling would generate temperature dependence of the KIEs according to the Bell theory, such that the isotopic activation-energy difference was larger than expected for the KIE magnitude but combined with a compensating value of $A^H/A^D < 1$. Therefore, Kwart[133–137] concluded that tunneling was not the origin of the temperature-independent KIEs just described. Indeed since most of the reactions studied by Kwart do not proceed via linear but via nonlinear transition states (Scheme 5) Kwart supposed, basically empirically, that temperature-independent H/D kinetic isotope effects must be associated with nonlinear H-transfer transition states. It was even argued[137,138] that the suggestion of a nonlinear transition state in the case of the 1,5-sigmatropic shift of pentadiene (Scheme 4b) for which temperature-dependent KIE had been observed[131] was incorrect. However, the nonlinear transition-state hypothesis was soon shown to be wrong by McLennan *et al.*[139,140] for the H-shift in pentadiene and by Anhede *et al.*[141] for the intramolecular proton transfer in mono-protonated methylenediamine.

It seems that the puzzle of Kwart's discovery that temperature-independent KIEs can arise in small-molecule reactions has not yet been solved. There is certainly no reason for doubting the reliability of the experimental work. The results for model systems and enzymes reviewed in the previous sections do, however, now suggest a solution to this problem in terms of tunneling.

In Scheme 6 we compare schematically the reaction pathway of hydrogen transfer from carbon to another heavy atom X. Scheme 6a refers to the case where only a small energy E_m or enthalpy ΔH is needed to form a linear pre-tunneling state exhibiting a reduced C..X distance. In this case the situation will be described in terms of Fig. 1a or 1b: the reaction will be dominated either by passage over the barrier, or by tunneling from excited vibrational levels. Hence, the kinetic isotope effects will be temperature-dependent. In this situation, the regime of temperature-independent tunneling can be reached only at very low temperatures.

By contrast, in Scheme 6b we consider the case where the formation of the pre-tunneling state involves a large energy. This is, for example, the case if C and X are part of the same molecular skeleton in such a structure that approximation of the two in a configuration appropriate for tunneling of H can only be attained by a large energy expenditure, or if the reaction centers are involved in interactions which have to be broken with a large energy expenditure in order to form the pre-tunneling state. The situation is similar to that found for BIM, OA5, and OA6 (Scheme 2). Here, the situation will be somewhere between those of Figs 1b and 1c. Even at high temperatures, the regime of temperature-independent kinetic isotope effects will be realized, i.e., the apparent energy of activation will be determined by the (isotope-independent) energy of formation of the pre-tunneling state rather than the isotope-dependent energy of formation of the transition state. Such a situation may prevail in the examples provided by the work from Kwart's laboratory.

CONCLUSIONS

We come to the following conclusions from this work. According to the Bell–Limbach model, Arrhenius curves of H-transfer reactions may be divided into three thermal zones, those of high, low, and intermediate temperatures. In the high-temperature zone, KIEs should correspond to the Bigeleisen–Wolfsberg theory[9–14] of isotope effects without the necessity of tunneling corrections. The slope of the Arrhenius curve is determined by the energy of formation of the transition state and the kinetic isotope effects are temperature dependent. In the low-temperature zone, the slope of the Arrhenius curve is determined by the energy or enthalpy of formation of the pre-tunneling state from which the reaction proceeds by tunneling. The pre-tunneling state is formed via isotope-insensitive heavy-atom motions leading to temperature-independent kinetic isotope effects. If the energy of formation of the pre-tunneling state is sufficiently large, the low-temperature zone may dominate even at room temperature. In the intermediate-temperature zone, the reaction proceeds via tunneling from vibrational states located somewhere between the pre-tunneling state and the transition state, rather than from the ground vibrational state of the pre-tunneling state. Here, the kinetic isotope effects are temperature dependent because the vibrational states will differ in energy for the two isotopic molecules.

The size of the kinetic H/D isotope effects arising from tunneling within the pre-tunneling state is reduced by heavy-atom tunneling during the H transfer. Such contributions are likely to be particularly small for hydrogen-atom transfers, where the transfer of the neutral atom will be accompanied by only minimal changes in polar interactions and thus minimal heavy-atom motion. Then the isotope effects could be quite large. In cases where H transfer is associated with single–double bond conversions, or by large changes in polar interactions requiring environmental reorganization, the associated heavy-atom motions may make the effective tunneling mass larger and reduce the magnitude of the isotope effects.

We consider that several phenomena can increase the energy of formation of a pre-tunneling state and thus should increase the likelihood of temperature-independent isotope effects even at relatively high temperatures. These are

(i) hydrogen bonding or coordination of the donor or acceptor atoms to molecules or molecular groups in the reactant state, if these interactions must be broken to allow the formation of the pre-tunneling state;
(ii) occurrence of an energetic intermediate on the reaction pathway into which tunneling takes place from the reactant state, so that the energy of formation of the pre-tunneling state must be sufficient that tunneling can occur from its vibrational ground state or low-lying vibrational excited states directly into the intermediate state.
(iii) major reorganization of a molecular skeleton is necessary in order to bring into approximation the heavy-atom frameworks involved in the hydrogen transfer, a process which could involve excitation of particular vibrational states.

From the measurement of Arrhenius curves alone it is not possible to obtain information about *which* heavy-atom motions are required for the reaction to occur. This is a particular problem in the discussion of the mechanism of enzymes where a combination of several phenomena may be responsible for the formation of the pre-tunneling state. Finally, the old problem of temperature-independent kinetic isotope effects in the case of hydrogen transfers in small molecules can easily be explained by the occurrence of high-energy pre-tunneling states.

Acknowledgements

This research was supported by the Deutsche Forschungsgemeinschaft, Bonn, and the Fonds der Chemischen Industrie (Frankfurt). HHL is indebted to Prof. Maurice Kreevoy, Minneapolis, Minnesota, USA, and Prof. G. S. Denisov, St. Petersburg, Russian Federation for stimulating discussions over three decades. The authors also thank Prof. G. S. Denisov for carefully reading the manuscript, and for his helpful comments. They are also grateful to the colleagues just named, as well as to the Alexander von Humboldt-Stiftung, Bonn-Bad Godesberg, for the support of our collaboration.

REFERENCES

[1] F. Hund, *Z. Phys.* **1927**, *43*, 805–826.
[2] G. Gamow, *Z. Phys.* **1928**, *51*, 204–212.
[3] R. P. Bell, *Proc. Roy. Soc. London Ser. A* **1933**, *139*, 466–474.
[4] R. P. Bell, *Proc. Roy. Soc. London Ser. A* **1935**, *148*, 241–250.
[5] R. P. Bell, *Proc. Roy. Soc. London Ser. A* **1936**, *154*, 414–429.
[6] R. P. Bell, *Trans. Faraday Soc.* **1938**, *34*, 229–236.
[7] R. P. Bell, O. M. Lidwell, *Proc. Roy. Soc. London Ser. A* **1940**, *176*, 114–121.
[8] R. P. Bell, *Adv. Catalys.* **1952**, *4*, 151–210.
[9] J. Bigeleisen, *J. Chem. Phys.* **1949**, *17*, 675–678.
[10] J. Bigeleisen, M. Wolfsberg, *J. Chem. Phys.* **1953**, *21*, 1972–1974.
[11] J. Bigeleisen, *J. Chem. Phys.* **1955**, *23*, 2264–2267.
[12] J. Bigeleisen, M. Wolfsberg, *Adv. Chem. Phys.* **1958**, *1*, 15–76.
[13] M. Wolfsberg, *Acc. Chem. Res.* **1972**, *5*, 225–233.
[14] L. Melander, W. H. Saunders, *Reaction Rates of Isotopic Molecules*, Krieger, Malabar, FL, **1987**.
[15] S. Glasstone, J. Laidler, H. Eyring, *The Theory of Rate Processes*, McGraw-Hill Book Company, Inc., New York, **1941**.
[16] G. Wentzel, *Z. Phys.* **1926**, *38*, 518–529.
[17] H. A. Kramers, *Z. Phys.* **1926**, *39*, 828–840.
[18] L. Brillouin, *C. R. Acad. Sci* **1926**, *153*, 24–26.
[19] R. P. Bell, *The Proton in Chemistry*, 2nd edn, Chapman and Hall, London, **1973**.
[20] R. P. Bell, *The Tunnel Effect in Chemistry*, Chapman and Hall, London, **1980**.
[21] *Proton Transfer Reactions*, (Eds.: E. Caldin, V. Gold), Chapman and Hall, London, **1975**.
[22] *Isotope Effects in the Biological and Chemical Sciences*, (Eds.: A. Kohen, H. H. Limbach), Taylor & Francis, Boca Raton FL, **2005**.
[23] *Hydrogen Transfer Reactions*, Vols. *1–4* (Eds.: J. T. Hynes, J. Klinman, H. H. Limbach, R. L. Schowen), Wiley-VCH Weinheim, Germany, **2007**.
[24] Faraday Symposium 'Proton Transfer', *Faraday Symp. Chem. Soc.* **1975**, *10*, 1–169.
[25] Faraday Discussion No. 74 'Proton and Electron Transfer', *J. Chem. Soc. Faraday Disc.* **1982**, *74*, 1–413.
[26] H. H. Limbach, J. Manz, *Ber. Bunsenges. Phys. Chem.* **1998**, *102*, 289–291.
[27] G. Brunton, J. A. Gray, D. Griller, L. R. C. Barclay, K. U. Ingold, *J. Am. Chem. Soc.* **1978**, *100*, 4197–4200.
[28] D. Gerritzen, H. H. Limbach, *J. Am. Chem. Soc.* **1984**, *106*, 869–879.
[29] H. H. Limbach, W. Seiffert, *J. Am. Chem. Soc.* **1980**, *102*, 538–542.
[30] H. H. Limbach, J. M. Lopez, A. Kohen, *Phil. Trans. B (London)* **2006**, *361*, 1399–1415.
[31] H. H. Limbach, *Single and multiple hydrogen/deuterium transfer reactions in liquids and solids, in Hydrogen Transfer Reactions*, In Ref. 23, Vols. 1 and 2, Chapter 6, p. 135–221.
[32] J. Basran, S. Patel, M. J. Sutcliffe, N. S. Scrutton, *J. Biol. Chem.* **2001**, *276*, 6234–6242.
[33] N. Bruniche-Olsen, J. Ulstrup, *J. Chem. Soc. Faraday Trans. 1* **1979**, *75*, 205–226.
[34] E. D. German, A. M. Kuznetsov, R. R. Dogonadze, *J. Chem. Soc. Faraday Trans. 2* **1980**, *76*, 1128–1146.
[35] A. M. Kuznetsov, J. Ulstrup, *Can. J. Chem.* **1999**, *77*, 1085–1096.
[36] A. M. Kuznetsov, J. Ulstrup, *Proton transfer and proton conductivity in condensed matter environment*. In Ref. 22, Chapter 26 pp. 691–724.
[37] M. J. Knapp, K. Rickert, J. P. Klinman, *J. Am. Chem. Soc.* **2002**, *124*, 3865–3874.
[38] W. Siebrand, T. A. Wildman, M. Z. Zgierski, *J. Am. Chem. Soc.* **1984**, *106*, 4083–4089.
[39] W. Siebrand, T. A. Wildman, M. Z. Zgierski, *J. Am. Chem. Soc.* **1984**, *106*, 4089–4096.
[40] V. A. Benderskii, E. V. Vetoshkin, L. von Laue, H. P. Trommsdorff, *Chem. Phys.* **1997**, *219*, 143–160.
[41] V. A. Benderskii, E. V. Vetoshkin, S. Y. Grebenshchikov, L. von Laue, H. P. Trommsdorff, *Chem. Phys.* **1997**, *219*, 119–142.
[42] V. A. Benderskii, E. V. Vetoshkin, H. P. Trommsdorff, *Chem. Phys.* **1998**, *234*, 153–172.
[43] V. A. Benderskii, E. V. Vetoshkin, H. P. Trommsdorff, *Chem. Phys.* **1999**, *244*, 273–297.
[44] V. A. Benderskii, E. V. Vetoshkin, H. P. Trommsdorff, *Chem. Phys.* **1999**, *244*, 299–317.
[45] D. Truhlar, *Variational transition-state theory and multidimensional tunneling for simple and complex reactions in the gas phase, solids, liquids, and enzymes*. In Ref. 22, Chapter 22, pp. 579–620.
[46] Z. Smedarchina, W. Siebrand, A. Fernández-Ramos, *Kinetic isotope effects in multiple proton transfer*. In Ref. 22, Chapter 22, pp. 521–548.
[47] W. F. Rowe, R. W. Duerst, E. B. Wilson, *J. Am. Chem, Soc.* **1976**, *98*, 4021–4023.
[48] S. L. Baughcum, R. W. Duerst, W. F. Rowe, Z. Smith, E. B. Wilson, *J. Am. Chem. Soc.* **1981**, *103*, 6296–6303.
[49] S. L. Baughcum, Z. Smith, E. B. Wilson, R. W. Duerst, *J. Am. Chem. Soc.* **1984**, *106*, 2260–2265.
[50] R. L. Redington, R. L. Sams, *J. Phys. Chem. A* **2002**, *106*, 7494–7511.
[51] F. Madeja, M. Havenith, *J. Chem. Phys.* **2002**, *117*, 7162–7168.
[52] D. W. Firth, P. F. Barbara, H. P. Trommsdorff, *Chem.Phys.* **1989**, *136*, 349–360.
[53] A. J. Horsewill, *Progr. NMR Spect.* **2008**, *52*, 170–196.
[54] H. H. Limbach, G. Scherer, M. Maurer, B. Chaudret, *Ang. Chem.* **1992**, *104*, 1414–1417. *Ang. Chem. Int. Ed. Engl.* **1992**, *31*, 1369–1372.
[55] H. H. Limbach, S. Ulrich, G. Buntkowsky, S. Gründemann, S. Sabo-Etienne, B. Chaudret, G. J. Kubas, J. Eckert, *J. Am. Chem. Soc.* **1998**, *120*, 7929–7943.
[56] J. Brickmann, H. Zimmermann, *Ber. Bunsenges. Phys. Chem.* **1966**, *70*, 157–165.
[57] J. Brickmann, H. Zimmermann, *Ber. Bunsenges. Phys. Chem.* **1966**, *70*, 521–524.
[58] J. Brickmann, H. Zimmermann, *Ber. Bunsenges. Phys. Chem.* **1967**, *71*, 160–164.
[59] J. Brickmann, H. Zimmermann, *J. Chem. Phys.* **1969**, *50*, 1608–1618.
[60] O. Brackhagen, Ch. Scheurer, R. Meyer, H. H. Limbach, *Ber. Bunsenges. Phys. Chem.* **1998**, *102*, 303–316.
[61] H. H. Limbach, G. Buntkowsky, J. Matthes, S. Gründemann, T. Pery, B. Walaszek, B. Chaudret, *ChemPhysChem.* **2006**, *7*, 551–554.
[62] G. Buntkowsky, B. Walaszek, A. Adamczyk, Y. Xu, H. H. Limbach, B. Chaudret, *Phys. Chem. Chem. Phys.* **2006**, *8*, 1929–1935.
[63] M. Eigen, *Angew. Chem. Int. Ed. Engl.* **1964**, *3*, 1–23.
[64] L. Pauling, *J. Am. Chem. Soc.* **1947**, *69*, 542–553.
[65] I. D. Brown, *Acta Cryst.* **1992**, *B48*, 553–572.
[66] T. Steiner, *J. Chem. Soc. Chem. Commun.* **1995**, 1331–1332.
[67] T. Steiner, *J. Phys. Chem. A* **1998**, *102*, 7041–7052.
[68] T. Steiner, *Angew. Chem. Int. Ed. Engl.* **2002**, *41*, 48–76.
[69] H. H. Limbach, G. S. Denisov, N. S. Golubev, *Hydrogen bond isotope effects studied by NMR*. In Ref. 22, Chapter 7, pp. 193–252.
[70] H. S. Johnston, *Gas Phase Reaction Rate Theory. Modern Concepts in Chemistry*, The Ronald Press Company, New York, **1966**.
[71] D. G. Truhlar, *J. Am. Chem. Soc.* **1972**, *94*, 7584–7586.
[72] N. Agmon, *Chem. Phys. Lett.* **1977**, *45*, 343–345.
[73] H. H. Limbach, P. M. Tolstoy, N. Pérez-Hernández, J. Guo, I. G. Shenderovich, G. S. Denisov, *Israel J. Chem.* **2009**, *49*, 199–216. Supplement, ibid. S1-S36.
[74] M. Ramos, I. Alkorta, J. Elguero, N. S. Golubev, G. S. Denisov, H. Benedict, H. H. Limbach, *J. Phys. Chem. A* **1997**, *101*, 9791–9800.
[75] J. M. Lopez, F. Männle, I. Wawer, G. Buntkowsky, H. H. Limbach, *Phys. Chem. Chem. Phys.* **2007**, *9*, 4498–4513.
[76] H. H. Limbach, M. Pietrzak, H. Benedict, P. M. Tolstoy, N. S. Golubev, G. S. Denisov, *J. Mol. Struct.* **2004**, *706*, 115–119.
[77] H. H. Limbach, M. Pietrzak, S. Sharif, P. M. Tolstoy, I. G. Shenderovich, S. N. Smirnov, N. S. Golubev, G. S. Denisov, *Chem. Eur. J.* **2004**, *10*, 5195–5204.

[78] K. F. Wong, T. Selzer, S. J. Benkovic, S. Hammes-Schiffer, *Proc. Natl Acad. Sci. USA* **2005**, *102*, 6807–6812.
[79] R. A. Marcus, *J. Chem. Phys.* **1966**, *45*, 4493–4499.
[80] A. I. Prokofiev, N. N. Bubnov, S. P. Solodovnikov, M. I. Kabachnik, *Tetrahedron Lett.* **1973**, 2479–2480.
[81] N. N. Bubnov, S. P. Solodovnikov, A. I. Prokofiev, M. I. Kabachnik, *Russ. Chem. Rev.* **1978**, *47*, 549–571.
[82] K. Loth, F. Graf, H. Günthardt, *Chem. Phys.* **1976**, *13*, 95–113.
[83] H. H. Limbach, D. Gerritzen, *Faraday Discuss. Chem. Soc.* **1982**, *74*, 279–296.
[84] S. F. Bureiko, G. S. Denisov, N. S. Golubev, I. Y. Lange, *React. Kinet. Catal. Lett.* **1979**, *11*, 35–38.
[85] A. Fernández-Ramos, Z. Smedarchina, J. Rodríguez-Otero, *J. Chem. Phys.* **2001**, *114*, 1567–1574.
[86] D. B. Northrop, *Acc. Chem. Res.* **2001**, *34*, 790–797.
[87] H. H. Limbach, J. Hennig, D. Gerritzen, H. Rumpel, *Faraday Discuss. Chem. Soc.* **1982**, *74*, 229–243.
[88] M. Schlabach, B. Wehrle, H. Rumpel, J. Braun, G. Scherer, H. H. Limbach, *Ber. Bunsenges. Phys. Chem.* **1992**, *96*, 821–833.
[89] B. Wehrle, H. H. Limbach, M. Köcher, O. Ermer, E. Vogel, *Ang. Chem. Int. Ed. Engl.* **1987**, *26*, 934–936.
[90] J. Braun, M. Schlabach, B. Wehrle, M. Köcher, E. Vogel, H. H. Limbach, *J. Am. Chem. Soc.* **1994**, *116*, 6593–6604.
[91] J. Braun, H. H. Limbach, P. G. Williams, H. Morimoto, D. Wemmer, *J. Am. Chem. Soc.* **1996**, *118*, 7231–7232.
[92] T. J. Butenhoff, C. B. Moore, *J. Am. Chem. Soc.* **1988**, *110*, 8336–8341.
[93] J. Braun, C. Hasenfratz, R. Schwesinger, H. H. Limbach, *Ang. Chem.* **1994**, *106*, 2302–2304. *Ang. Chem. Int. Ed. Engl.* **1994**, *33*, 2215–2217.
[94] J. Braun, R. Schwesinger, P. G. Williams, H. Morimoto, D. E. Wemmer, H. H. Limbach, *J. Am. Chem. Soc.* **1996**, *118*, 11101–11110.
[95] H. Rumpel, H. H. Limbach, *J. Am. Chem. Soc.* **1989**, *111*, 5429–5441.
[96] G. Otting, H. Rumpel, L. Meschede, G. Scherer, H. H. Limbach, *Ber. Bunsenges. Phys. Chem.* **1986**, *90*, 1122–1129.
[97] G. Scherer, H. H. Limbach, *J. Am. Chem. Soc.* **1989**, *111*, 5946–5947.
[98] G. Scherer, H. H. Limbach, *J. Am. Chem. Soc.* **1994**, *116*, 1230–1239.
[99] G. Scherer, H. H. Limbach, *Croat. Chem. Acta* **1994**, *67*, 431–440.
[100] H. Rumpel, H. H. Limbach, G. Zachmann, *J. Phys. Chem.* **1989**, *93*, 1812–1818.
[101] L. Meschede, D. Gerritzen, H. H. Limbach, *Ber. Bunsenges. Phys. Chem.* **1988**, *92*, 469–485.
[102] H. H. Limbach, L. Meschede, G. Scherer, *Z. Naturforsch.* **1989**, *44a*, 459–471.
[103] L. Meschede, H. H. Limbach, *J. Phys. Chem.* **1991**, *95*, 10267–10280.
[104] F. Männle, I. Wawer, H. H. Limbach, *Chem. Phys. Lett.* **1996**, *256*, 657–662.
[105] R. Anulewicz, I. Wawer, T. M. Krygowski, F. Männle, H. H. Limbach, *J. Am. Chem. Soc.* **1997**, *119*, 12223–12230.
[106] J. M. Lopez del Amo, U. Langer, V. Torres, G. Buntkowsky, H. M. Vieth, M. Pérez-Torralba, D. Sanz, R. M. Claramunt, J. Elguero, H. H. Limbach, *J. Am. Chem. Soc.* **2008**, *130*, 8620–8632.
[107] R. M. Claramunt, D. Sanz, S. H. Alarcón, M. Pérez-Torralba, J. Elguero, C. Foces-Foces, M. Pietrzak, U. Langer, H. H. Limbach, *Angew. Chem. Int. Ed. Engl. 40*, 420–423.
[108] M. Pietrzak, H. H. Limbach, M. Perez-Torralba, D. Sanz, R. M. Claramunt, J. Elguero, *Magn. Reson. Chem.* **2001**, *39*, S100–S108.
[109] C. G. Hoelger, H. H. Limbach, *J. Phys. Chem.* **1994**, *98*, 11803–11810.
[110] U. Langer, L. Latanowicz, Ch. Hoelger, G. Buntkowsky, H. M. Vieth, H. H. Limbach, *Phys. Chem. Chem. Phys.* **2001**, *3*, 1446–1458.
[111] T. Vangberg, A. Ghosh, *J. Phys. Chem. B* **1997**, *101*, 1496–1497.
[112] D. K. Maity, R. L. Bell, T. N. Truong, *J. Am. Chem. Soc.* **2000**, *122*, 897–906.
[113] M. H. Glickman, J. S. Wiseman, J. P. Klinman, *J. Am. Chem. Soc.* **1994**, *116*, 793–794.
[114] M. H. Glickman, J. P. Klinman, *Biochemistry* **1995**, *34*, 14077–14092.
[115] M. H. Glickman, J. P. Klinman, *Biochemistry* **1996**, *35*, 12882–12892.
[116] M. H. Glickman, S. Cliff, M. Thiemens, J. P. Klinman, *J. Am. Chem. Soc.* **1997**, *119*, 11357–11361.
[117] T. Jonsson, M. H. Glickman, S. J. Sun, J. P. Klinman, *J. Am. Chem. Soc.* **1996**, *118*, 10319–10320.
[118] K. W. Rickert, J. P. Klinman, *Biochemistry* **1999**, *38*, 12218–12228.
[119] A. Kohen, R. Cannio, S. Bartolucci, J. P. Klinman, *Nature* **1999**, *399*, 496–499.
[120] K. Anandarajah, K. B. Schowen, R. L. Schowen, *Z. Phys. Chem.* **2008**, *222*, 1333–1347.
[121] A. Kohen, J. P. Klinman, *Chem. Biol.* **1999**, *6*, R191–R198.
[122] A. Kohen, J. P. Klinman, *J. Am. Chem. Soc.* **2000**, *122*, 10738–10739.
[123] Z. X. Liang, T. Lee, K. A. Resing, N. G. Ahn, J. P. Klinman, *Proc. Natl Acad. Sci. USA* **2004**, *101*, 9556–9561.
[124] E. F. Caldin, C. J. Wilson, *J. Chem. Soc. Faraday Symp.* **1975**, *10*, 121–131.
[125] E. F. Caldin, S. Mateo, *J. Chem. Soc. Faraday Trans. 1*, **1975**, *71*, 1876–1904.
[126] E. F. Caldin, S. Mateo, P. Warrick, *J. Am. Chem. Soc.* **1981**, *103*, 202–204.
[127] O. Rogne, *J. Chem. Soc., Chem. Commun.* **1977**, 695–696.
[128] J. H. Blanch, O. Rogne, *J. Chem. Soc., Faraday Trans. 1* **1978**, *74*, 1254–1262.
[129] O. Rogne, *Acta Chem. Scand., Ser. A* **1978**, *32*, 559–563.
[130] A. J. Kresge, M. F. Powell, *J. Am. Chem. Soc.* **1981**, *103*, 201–202.
[131] W. R. Roth, J. König, *Liebigs Ann. Chem.* **1966**, *699*, 24–36.
[132] H. Kwart, M. C. Latimore, *J. Am. Chem. Soc.* **1971**, *93*, 3770–3771.
[133] H. Kwart, T. J. George, R. Louw, W. Ultee, *J. Am. Chem. Soc.* **1978**, *100*, 3927–3928.
[134] H. Kwart, A. Gaffney, *J. Org. Chem.* **1983**, *48*, 4502–4508.
[135] H. Kwart, A. Gaffney, K. A. Wilk, *J. Org. Chem.* **1983**, *48*, 4509–4513.
[136] H. Kwart, A. Gaffney, K. A. Wilk, *J. Chem. Soc., Perkin Trans. 2* **1984**, 565–568.
[137] H. Kwart, M. W. Brechbiel, R. M. Acheson, D. C. Ward, *J. Am. Chem. Soc.* **1982**, *104*, 4671–4672.
[138] H. Kwart, *Acc. Chem. Res.* **1982**, *15*, 401–408.
[139] D. J. McLennan, P. M. Gill, *J. Am. Chem. Soc.* **1985**, *107*, 2971–2972.
[140] D. J. McLennan, P. M. Gill, *Israel J. Chem.* **1985**, *26*, 378–386.
[141] B. Anhede, N. A. Bergman, *J. Am. Chem. Soc.* **1984**, *106*, 7634–7636.

